Diversification of small RNA pathways underlies germline RNAi incompetence in wild *C. elegans* strains

Han Ting Chou[1], Francisco Valencia[1], Jacqueline C. Alexander[1], Avery Davis Bell[1], Diptodip Deb[1], Daniel A. Pollard[2], Annalise B. Paaby[1,3]

1. School of Biological Sciences, Georgia Institute of Technology, Atlanta, GA, USA
2. Biology Department, Western Washington University, Bellingham, WA, USA
3. Correspondence: paaby@gatech.edu

ABSTRACT

The discovery that experimental delivery of dsRNA can induce gene silencing at target genes revolutionized genetics research, by both uncovering essential biological processes and creating new tools for developmental geneticists. However, wild-type *C. elegans* strains vary dramatically in their response to exogenous RNAi, challenging our characterization of RNAi in the lab relative to its activity and significance in nature. Here, we investigate why some strains fail to mount a robust RNAi response to germline targets. We observe diversity in mechanism: in some strains, the response is stochastic, either on or off among individuals, while in others the response is consistent but delayed. Increased activity of the Argonaute PPW-1, which is required for germline RNAi in the laboratory strain N2, rescues the response in some strains, but dampens it further in others. Across strains, we observe variability in expression of known RNAi genes and strain-specific instances of pseudogenization and allelic divergence. Our results support the conclusions that Argonautes share overlapping functions, that germline RNAi incompetence is strain-specific but likely caused by genetic variants at common genes, and that RNAi pathways are evolving rapidly and dynamically. This work expands our understanding of RNAi by identifying conserved and variable pathway components, and it offers new access into characterizing gene function, identifying pathway interactions, and elucidating the biological significance of RNAi.

32 **INTRODUCTION**

33

34 The landscape of molecular and developmental genetics in *C. elegans* has been transformed by
35 the ability to silence genes by feeding worms *E. coli* bacteria engineered to express RNA
36 matching worm gene targets (*Kamath et al., 2003; Rual et al., 2004; Timmons & Fire, 1998*). This
37 tool emerged from the seminal discovery that double stranded RNA induces gene suppression
38 (*Fire et al., 1998*). The discovery, awarded the Nobel prize in 2006, launched research into new
39 mechanisms of gene regulation and led to the eventual characterization of the microRNA
40 (miRNA), short interfering RNA (siRNA), and PIWI-interacting (piRNA) pathways. These
41 pathways overlap in gene set and molecular mechanisms, but differ in origination of the RNA
42 trigger molecules and mediate processes as diverse as gene regulation in cell growth and tissue
43 differentiation, adaptive immunity against pathogens, transgenerational epigenetic inheritance,
44 and germline defense against transposons (*Grishok, 2013; Wilson & Doudna, 2013*). Many of the
45 genes that encode this machinery are shared across plants, animals, and fungi, and appear deeply
46 conserved within the eukaryotic lineage (*Shabalina & Koonin, 2008; Wynant et al., 2017*).

47

48 The umbrella term "RNA interference" (RNAi) refers to the general mechanism of gene
49 silencing via dsRNA, and those shared pathways that mediate it across diverse processes (*Yigit et*
50 *al., 2006*). The complexity of RNAi is reflected in the many overlapping ways its activity can be
51 classified: by endogenous biogenesis of the small RNA trigger versus exogenous or
52 environmental delivery; as nuclear RNAi, which induces transcriptional gene silencing, versus
53 post-transcriptional cytoplasmic RNAi; as a phenomenon localized to the cell in which the
54 dsRNA trigger occurs, versus systemic RNAi, which involves transport mechanisms; by
55 silencing genes expressed in the soma versus targets in the germline. These classifications
56 emerged as experiments revealed distinct genetic mechanisms among them. However, all RNAi
57 processes silence complementary mRNA targets via the association of small RNAs with
58 Argonaute effector proteins (*Wilson & Doudna, 2013*).

59

60 The Argonaute superfamily includes the ancient AGO proteins; the PIWI Argonautes, which are
61 conserved in animals; and in *C. elegans*, the WAGO proteins, an expanded clade of Argonautes
62 specific to nematodes (*Youngman & Claycomb, 2014*). The expansion of Argonautes in nematodes
63 may underlie the extraordinary diversification of worms across environments, perhaps having

64 enabled adaptations associated with environmental sensing, parasitism, and immunity (*Buck &*
65 *Blaxter, 2013*). Several viruses that infect *C. elegans* and other *Caenorhabditis* species have been
66 discovered, notably in isolates with defective RNAi, and antiviral immunity shows a clear
67 association with an active RNAi response (*Félix et al., 2011; Sarkies et al., 2013; Schott et al., 2005;*
68 *Wilkins et al., 2005; Yigit et al., 2006*). Yet, experimental RNAi appears partially distinct from the
69 antiviral response, as variation in RNAi sensitivity does not completely correlate with immunity,
70 and the systemic and transgenerational properties of RNAi are not observed in viral infection
71 (*Ashe et al., 2013, 2015; Félix et al., 2011*). The adaptive functionalization of RNAi genes and
72 pathways across processes emphasizes the essentiality of RNAi, but our understanding of its
73 biological significance remains incomplete.
74
75 Although *C. elegans* sits at the epicenter of expansive research programs into gene silencing by
76 small RNAs, worms vary significantly in capacity for RNAi. Across the *Caenorhabditis* genus,
77 some species, like *C. elegans*, will mount an RNAi response upon environmental exposure to
78 dsRNA, but some require injection of the trigger, indicating a deficiency in spreading the
79 response systemically, and some show no response (*Nuez & Félix, 2012; Winston et al., 2007*).
80 Within *C. elegans*, wild-type strains also vary. The universal laboratory strain N2 is robustly
81 sensitive to RNAi, but RNAi response varies quantitatively among other isolates, for targets in
82 both the germline and soma, and some strains show incompetence for RNAi by feeding or
83 injection (*Félix et al., 2011; Paaby et al., 2015; Tijsterman et al., 2002*). For example, the Hawaiian
84 isolate CB4856 appears largely insensitive to RNAi in the germline. Its insensitivity has been
85 mapped to the *ppw-1* locus, which encodes a WAGO Argonaute, and is presumably explained by
86 a single nucleotide deletion producing a frameshift and early stop in the first half of the transcript
87 (*Tijsterman et al., 2002*). To date, this is the only causal variant identified for natural differences in
88 RNAi, though genetic mapping crosses indicate that the weak germline RNAi in CB4856 is
89 genetically complex and likely involves additional factors (*Elvin et al., 2011; Pollard & Rockman,*
90 *2013; Tijsterman et al., 2002*).
91
92 In this study, we investigate the genetic basis of germline RNAi deficiency in wild *C. elegans*
93 strains. Earlier work employing a high throughput RNAi assay targeting maternal-effect
94 embryonic genes in wild isolates revealed a spectrum of germline RNAi competence, from
95 strains with negligible response on most targets to several that were more sensitive than the

96 laboratory strain N2 (*Paaby et al., 2015*). Here, we evaluate strains with negligible germline
97 RNAi, with the goals of, firstly, accurately measuring RNAi activity, and secondly,
98 characterizing mechanisms of failure. We evaluate the response at the organismal, cellular, and
99 gene expression levels, and observe distinct variations in how and why germline RNAi fails. We
100 also observe meaningful allelic variation at known RNAi genes in these strains and in the *C.*
101 *elegans* population at large, suggesting that selection has diversified RNAi activity at both the
102 sequence and functional levels.
103
104 **RESULTS**
105
106 **Germline RNAi varies in expressivity and penetrance over reproductive age and among**
107 **genotypes**
108
109 Previous work has shown that the WAGO Argonaute PPW-1 is essential for germline RNAi. In
110 the RNAi-responsive laboratory strain N2, a 1.5kb intragenic deletion spanning the PAZ and
111 PIWI domains in *ppw-1* (*pk1425*) eliminates germline RNAi by feeding (*Tijsterman et al., 2002;*
112 *Yigit et al., 2006*). Germline RNAi deficiency in the Hawaiian isolate CB4856, which is one of the
113 most insensitive wild-type strains so far observed (*Paaby et al., 2015*), has been mapped to the
114 *ppw-1* locus, which in CB4856 includes a frameshift and early stop upstream of the critical PAZ
115 and PIWI domains (*Elvin et al., 2011; Pollard & Rockman, 2013; Tijsterman et al., 2002*).
116
117 We measured the germline RNAi responses of N2, N2 carrying the 1.5kb deletion allele (N2^{ppw-}
118 $^{1(del)}$), CB4856, and QX1211, a wild isolate that exhibits germline RNAi incompetence similar to
119 CB4856 (*Paaby et al., 2015*). We targeted the maternal-effect, embryonic-required genes *par-1*
120 and *pos-1*, which have commonly been used to measure germline RNAi (*Elvin et al., 2011;*
121 *Pollard & Rockman, 2013; Tijsterman et al., 2002*), by feeding hermaphrodites *E. coli* expressing
122 target dsRNA; we then counted dead embryos in the next generation. Using a conventional
123 approach, in which hermaphrodites are pooled on plates and offspring are scored in a window of
124 relatively early egg-laying (*Kamath et al., 2001; Pollard & Rockman, 2013*), we observed high
125 lethality for N2 and very low or negligible lethality in the three low-response strains (Figure 1A).
126

127 However, following an initial trigger, amplification within the RNAi response can induce strong
128 effects later (*Billi et al., 2014*), and continual exposure to RNAi by feeding also means that
129 individuals ingest increasing numbers of trigger molecules as they age. To evaluate whether and
130 how the RNAi response changes over time within individual animals, we scored the penetrance
131 of embryonic lethality over the entire reproductive lifespan of egg-laying hermaphrodites. In this
132 assay we used *par-1*, which provides the more sensitive readout since it is not as lethal. Here, N2
133 exhibited complete lethality in all but the earliest offspring, while the low-response strains
134 showed unique patterns of a slow or incomplete response (Figure 1B). Nearly all N2$^{ppw\text{-}1(del)}$
135 embryos hatched, including late-age embryos, indicating that the loss of *ppw-1* is not
136 compensated by any other genes in the N2 background. However, embryonic lethality increased
137 over time in CB4856. This suggests that the frameshift lesion in CB4856 may not be a null
138 allele, permitting some PPW-1 activity; or that other genes in the CB4856 background may
139 partially compensate for the loss of PPW-1, promoting a delayed RNAi response.
140
141 To distinguish between these alternatives, we tested a strain carrying the CB4856-derived allele
142 of *ppw-1* (*pk2505*) introgressed into the N2 background (N2$^{ppw\text{-}1(CB4856)}$). This strain produced an
143 intermediate response: more responsive than CB4856, especially in the earliest time interval, but
144 never as responsive as N2, even in late age (Figure 1B). This suggests that both explanations
145 matter. N2$^{ppw\text{-}1(CB4856)}$ is likely more responsive than CB4856 due to its N2 background,
146 consistent with previous reports that the *ppw-1* allele does not fully explain insensitivity in
147 CB4856 (*Pollard & Rockman, 2013; Tijsterman et al., 2002*). However, the stronger response of
148 N2$^{ppw\text{-}1(CB4856)}$ relative to N2$^{ppw\text{-}1(del)}$ suggests that the naturally-occurring frameshift mutation in
149 CB4856 is not as deficient as the 1.5kb deletion, or that additional polymorphisms within the
150 introgressed CB4856 interval modify the frameshift allele. This outcome would be consistent
151 with an earlier investigation of germline RNAi in CB4856, which implicates genetic complexity
152 in the *ppw-1* genome region (*Pollard & Rockman, 2013*).

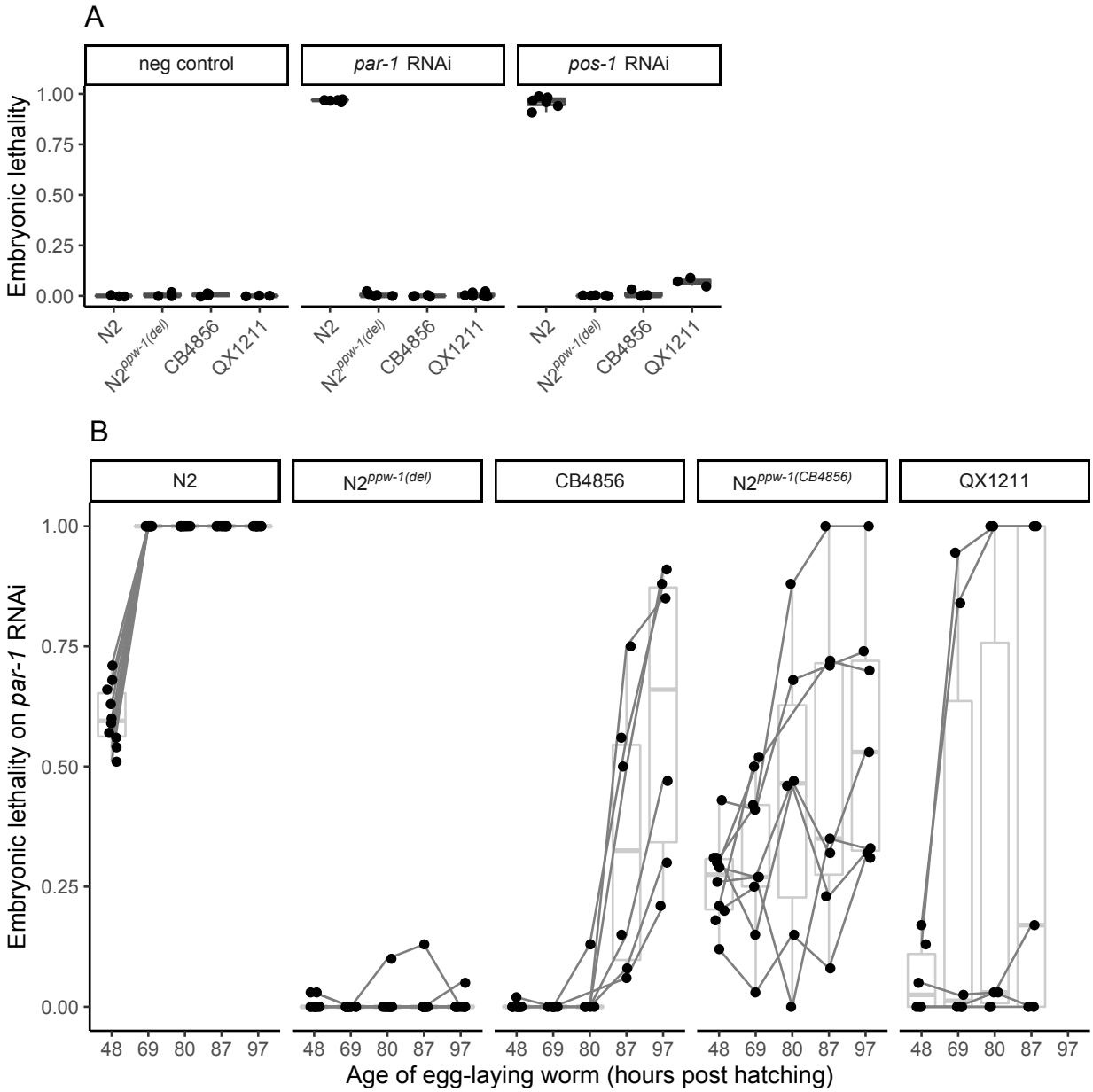

Figure 1. Embryonic lethality following RNAi against germline-expressed targets. (A) Hatched larvae and dead embryos laid in a 4-6hr window within the first 8hrs of egg-laying were scored for pooled hermaphrodites across replicate plates. (B) To assess the germline RNAi response over reproductive lifespan, embryonic lethality was scored for individuals. Each point represents the proportion of embryos laid on a plate by a single hermaphrodite that died in the given time interval. The data include all offspring of all hermaphrodite mothers; time intervals were chosen to space out the number of offspring per plate (~30-100); x-axis labels indicate the approximate midpoint of the time intervals. Connecting lines indicate the sequence of offspring plates for each individual. Embryonic lethality for all strains on the negative control empty vector was negligible (data not shown).

164 QX1211 exhibited low lethality in the earliest laid embryos, but subsequently produced a
165 bimodal response, suggesting that RNAi in this strain is either "on" or "off" in individual
166 animals. Notably, the response does not appear to increase in the "off" individuals over time;
167 instead, they exhibit negligible embryonic lethality over the entire reproductive period. These
168 findings show that wild isolates CB4856 and QX1211 are capable of germline RNAi, though
169 their responses are limited. Further, they show distinct patterns of activity: in CB4856, the
170 response is delayed and incomplete; in QX1211, it is partially delayed, with higher expressivity
171 and variable penetrance.
172
173 **Target transcript knockdown confirms distinct RNAi responses across strains**
174
175 The use of an end-point phenotype to read out the RNAi response, in this case embryonic
176 lethality, cannot capture activity at the molecular or cellular level. So, to assess the RNAi
177 response with high spatial and temporal resolution within embryos, we used single-molecule
178 fluorescence *in situ* hybridization (smFISH) to visualize transcripts of germline RNAi targets.
179 Since smFISH visualizes individual molecules via hybridization of dozens of oligonucleotide
180 probes, which in aggregate produce a detectable fluorescent spot (*Raj et al., 2008*), it captures
181 signals from intact RNAs, not those degraded by RNAi.
182
183 We examined *par-1* transcript levels in *par-1* RNAi-treated and -untreated embryos of N2,
184 CB4856 and QX1211. We collected embryos from gravid hermaphrodites in early reproductive
185 maturity, in a narrow two-hour window, to maximize precision in estimating the RNAi response.
186 At this timepoint, many *par-1* transcripts are degraded in RNAi-treated N2 embryos (Figure 2A-
187 B). Treated N2 embryos of this timepoint go on to show complete lethality, but in CB4856 and
188 QX1211, lethality is not yet penetrant (Figure 2C).
189
190 For all three strains, we observed robust expression of the target gene in untreated embryos. This
191 outcome diminishes the likelihood that the variable embryonic lethality we had observed was
192 driven by differences in native expression of the target gene, rather than differences in RNAi. In
193 RNAi-treated embryos, the transcript levels further confirm the distinct RNAi responses we
194 previously observed: N2 showed a steep drop in abundance, CB4856 showed no change, and

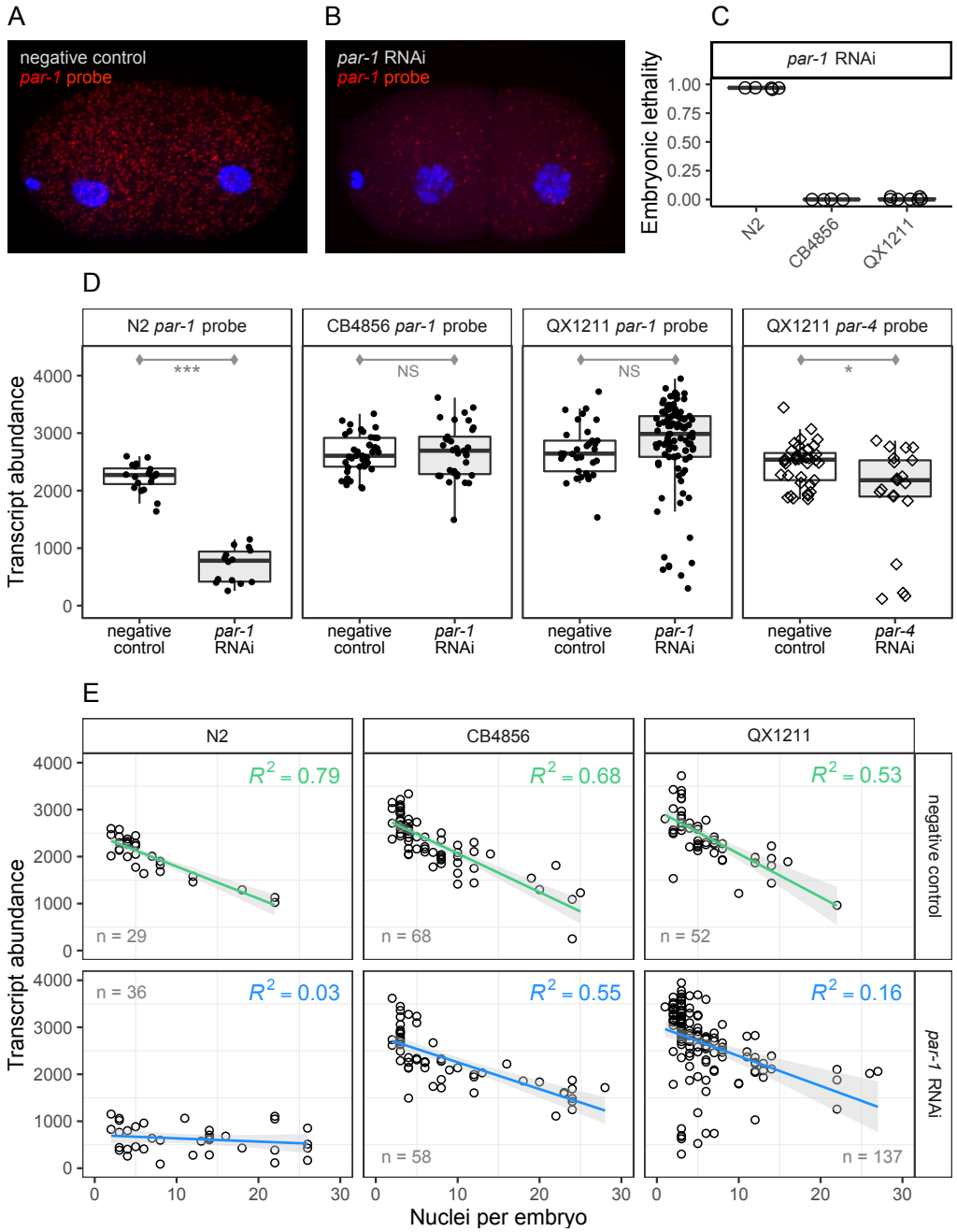

Figure 2. Transcript abundance in individual RNAi-treated and untreated embryos, visualized via single-molecule fluorescence in situ hybridization (smFISH). (A) - (B) Representative embryos are shown from strain N2, from a mother reared in the control condition or with RNAi against *par-1*; red spots indicate *par-1* transcripts and blue DAPI staining shows nuclei, which were used to identify embryo stage. (C) Embryonic lethality was simultaneously measured in matched samples. To limit variation due to reproductive age of the mothers, we collected embryos from a tightly controlled time window in early reproduction. (D) Transcript abundance for early stage embryos (up to four cells). (E) Transcript abundance for *par-1* for the same experiment, but now including later stage embryos with up to 30 nuclei. Green (negative control) and blue (RNAi treatment) lines indicate the linear regression of transcript counts onto embryonic stage; gray shading indicates the 90% confidence interval. For (D) and (E), each point represents one embryo. Significance levels (*t*-tests): p<0.001 (***), p<0.01 (**), p<0.05 (*).

208 QX1211 showed N2-like levels for some, but not most, embryos (Figure 2D). Specifically, in
209 early stage embryos (up to four cells), N2 shows a significant reduction in *par-1* transcript
210 abundance after *par-1* RNAi ($t=-16.34$, $df=32$, $p<0.001$), while CB4856 and QX1211 do not
211 ($t=0.41$, $df=56.31$, $p=0.684$ and $t=1.15$, $df=95.03$, $p=0.255$, respectively) (Figure 2D). However,
212 for CB4856, the variance in abundance is slightly higher for treated embryos than for control
213 embryos ($F=1.94$, $df=32,40$, $p=0.048$), which may represent the onset of an RNAi response. In
214 QX1211, the variance of treated embryos is substantially higher ($F=2.94$, $df=100,32$, $p<0.001$)
215 and is bimodally distributed, with low-abundance embryos at levels similar to N2. We observed
216 a similar pattern in QX1211 for a second germline target, *par-4*, in which treated embryos
217 showed a slight reduction in average abundance but substantial increase in variance ($t=-2.64$,
218 $df=24.20$, $p=0.014$ and $F=5.50$, $df=20,36$, $p<0.001$, respectively) (Figure 2D). These results,
219 which mirror the observation of on/off embryonic lethality in QX1211 (Figure 1B), are further
220 evidence that induction of RNAi can occur early but is stochastic within this strain.
221
222 To examine how transcript abundance changes with embryonic development across strains, we
223 evaluated embryos with up to 30 nuclei. In the control condition, we observed that *par-1*
224 transcripts decrease with embryonic stage (Figure 2E) (*Charles et al., 2021*), and that the rate of
225 decrease was consistent across strains (ANCOVA model comparison, $p=0.299$). However,
226 overall N2 exhibited significantly fewer *par-1* transcripts than either CB4856 or QX1211
227 ($p<0.001$). Thus, while we conclude that changes in transcript abundance between control and
228 treatment conditions (or lack thereof) are good indicators of an RNAi response, we cannot rule
229 out the possibility that differences in native gene expression between strains might also mediate
230 differences in apparent response for specific targets.
231
232 The strain-specific patterns of RNAi we observed in early-stage embryos (Figure 2D) persisted
233 across development (Figure 2E). We considered how transcript abundance changed between
234 treated and untreated embryos within each strain, after adjusting for embryo stage. For N2, most
235 of the variance in transcript abundance can be explained by treatment ($\omega^2=0.586$), then embryo
236 stage ($\omega^2=0.248$), then by the interaction between them ($\omega^2=0.059$) (ANCOVA model
237 comparison, $p<0.001$ for all). This makes sense, as transcripts are dramatically depleted in
238 RNAi-treated N2 embryos. For CB4856 and QX1211, however, the treatment condition explains
239 very little of the variance in transcript abundance ($\omega^2=0.010$, $p=0.043$ and $\omega^2=0.014$, $p=0.037$,

240 respectively). Instead, the variance observed for CB4856 is well explained by embryo stage
241 (ω^2=0.581, p<0.001) and minimally by the interaction (ω^2=0.017, p=0.012), consistent with the
242 conclusion that the RNAi response is negligible in CB4856 at this stage of germline
243 development. In QX1211, variance in transcript abundance is less well explained overall, since
244 incompleteness of the RNAi response adds noise to the transcript counts in treated QX1211
245 embryos (ω^2=0.208, p<0.001 for embryo stage and p=NS for the interaction).
246
247 **Reduced PPW-1 function explains weak germline RNAi response for some, but not all, low-**
248 **response strains**
249
250 We surveyed the several hundred wild isolates in the *Caenorhabditis elegans* Natural Diversity
251 Resource (CeNDR) database (*Cook et al., 2017*) and found that the naturally-occurring stop-
252 gain/frameshift mutation in *ppw-1* (*Tijsterman et al., 2002*) is unique to CB4856. Nevertheless, we
253 hypothesized that variation in PPW-1 activity might account for the observed differences in
254 germline RNAi among wild strains. To test whether reduction of PPW-1 function might be a
255 universal aspect of reduced germline RNAi, we performed complementation tests by crossing N2
256 wild-type and null alleles of *ppw-1* to seven wild isolates. We evaluated CB4856, QX1211, and
257 five additional strains, selected based on prior observations of weak germline RNAi (data not
258 shown) (*Paaby et al., 2015*) and representation of nucleotide diversity and divergence across the
259 global population (*Cook et al., 2017*).
260
261 We crossed each wild isolate to N2, which carries its native, wild-type copy of *ppw-1*, and also
262 to N2 carrying the *ppw-1* deletion allele (*pk1425*). But because N2 carries a sperm-delivered
263 toxin allele at *peel-1*, which causes genetic incompatibility with strains that do not carry the
264 linked zygotic antidote at *zeel-1* (*Seidel et al., 2008, 2011*), we generated a strain derived from N2
265 with both the *ppw-1* deletion and an allele of *peel-1* (*kah126*) that disables the toxin by a
266 frameshift insertion in the second exon ($N2^{ppw\text{-}1(del);peel\text{-}1}$). Use of this allele eliminates embryonic
267 lethality that would otherwise arise in the F2 generation, from F1 heterozygotes derived from
268 incompatible strains. The presence of this *peel-1* allele had no effect on our measured RNAi
269 response in either sensitive or resistant backgrounds (Figure 3A, Figure S1), so we used it in all
270 comparisons requiring the N2 background.

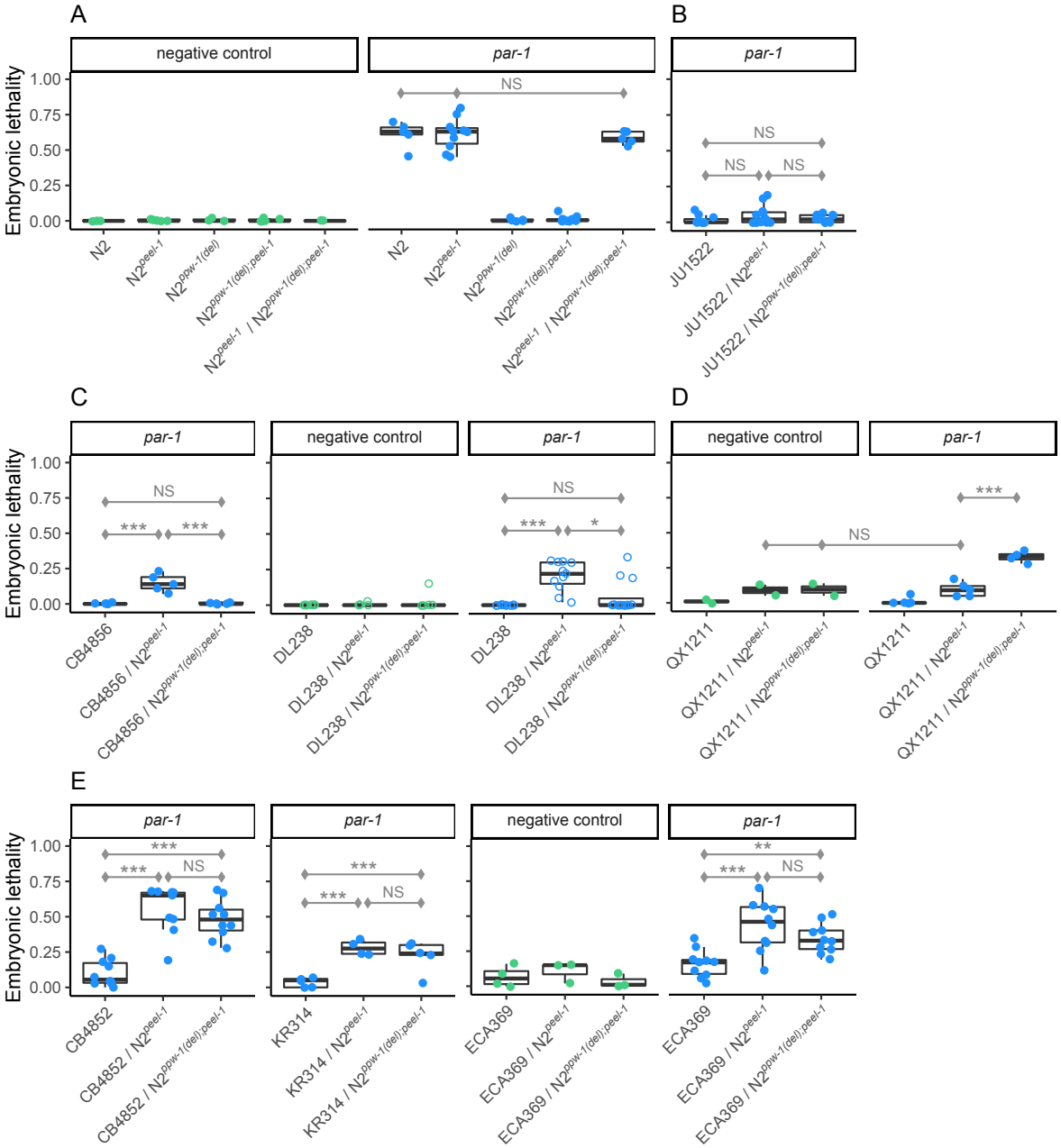

Figure 3. Complementation tests between seven wild isolates with low RNAi response and the RNAi-sensitive laboratory strain N2, with and without the *ppw-1* deletion allele. Response was measured by embryonic lethality following RNAi by feeding against the embryonic target *par-1*. (A) To circumvent embryonic lethality arising from the *peel-1*/*zeel-1* genetic incompatibility, we used a null allele of the sperm-delivered toxin *peel-1* in N2, which has no effect on RNAi in either the responsive (N2) or the resistant ($N2^{ppw\text{-}1(del)}$) backgrounds. A single copy of *ppw-1* is sufficient to fully restore the germline RNAi response in N2. (B) - (E) Complementation tests for seven wild isolates with weak germline RNAi, representing a diversity of genetic backgrounds. For DL238 (C), rather than the average across pooled hermaphrodites, each point represents the proportion of dead embryos from one individual; the overall pattern qualitatively replicates that which we observed in pooled hermaphrodites (Figure S2). For (B) - (E), embryonic lethality in the negative control condition is shown only when it was observed to be greater than zero. Significance levels (Tukey's contrasts): $p<0.001$ (***), $p<0.01$ (**), $p<0.05$ (*).

285 For each cross, we compared the response of the individual wild isolate to the two heterozygote
286 genotypes in the F1 generation, with and without the deletion at *ppw-1* inherited from the N2
287 chromosome. As previously, we induced *par-1* RNAi in the (F1) hermaphrodite germline and
288 measured embryonic lethality in the following generation. To avoid confounding differences in
289 developmental timing with variation in RNAi response, we scored all progeny from the first
290 15hrs of egg-laying from a small pool of hermaphrodites (~100-200 embryos) on each replicate
291 plate. Though N2 homozygous for the *ppw-1* deletion fails to exhibit an RNAi response, one
292 copy of wild-type *ppw-1* fully rescues it, indicating that *ppw-1* is haplo-sufficient, at least in the
293 N2 background (Figure 3A). Therefore, we reasoned that if weak RNAi response in the wild
294 isolates was a consequence of reduced PPW-1 activity, any restoration of RNAi response in the
295 F1 genotypes would be greater in the genotype with the functional N2 *ppw-1* allele.
296
297 Across the seven *C. elegans* isolates, we observed four distinct response patterns: (i) no rescue,
298 (ii) *ppw-1*-dependent rescue, (iii) *ppw-1*-dependent suppression, and (iv) *ppw-1*-independent
299 rescue. These results indicate that among wild-type strains, PPW-1 activity varies, PPW-1
300 activity differentially affects germline RNAi due to interaction with other varying factors, or
301 both. The results suggest that weak germline RNAi is multigenic within each strain, since in each
302 instance of rescue, the response was still lower than N2 levels, indicating the presence of factors
303 other than *ppw-1*.
304
305 (i) Strain JU1522 showed no rescue, i.e., no improved RNAi response in either F1 genotype
306 (Figure 3B). This outcome does not necessarily mean that weak RNAi in JU1522 is independent
307 of *ppw-1*, but it does indicate that none of the alleles that promote RNAi in N2, including *ppw-1*,
308 are haplo-sufficient to increase the response in the JU1522 background.
309
310 (ii) As expected, CB4856 exhibited *ppw-1*-dependent rescue: we observed a significantly
311 increased RNAi response when crossed to N2, but only in the background with the wild-type
312 *ppw-1* allele (Figure 3C). This is consistent with prior reports implicating *ppw-1* insufficiency as
313 a major cause of weak germline RNAi in this strain (*Pollard & Rockman, 2013; Tijsterman et al.,*
314 *2002*). Strain DL238 exhibited a similar pattern. However, replicate to replicate variation in
315 embryonic lethality was high in DL238 F1s, so we investigated whether this could be explained
316 by potentially stochastic induction of the RNAi response between individual worms. This

317 appears to be the case: tested individually, we observed that some hermaphrodites produced no
318 dead embryos and others over 30% (Figure 3C). Although DL238 does not carry the *pha-1*
319 zygotic antidote to a second genetic incompatibility, arising from the *sup-35* toxin carried by N2
320 (*Ben-David et al., 2017*) and for which we did not control, we saw only very weak penetrance of
321 this effect (Figure 3C).
322
323 (iii) Unexpectedly, QX1211 demonstrated *ppw-1*-dependent suppression: the heterozygote with
324 the *ppw-1* deletion allele exhibited a significant increase in embryonic lethality, implying that
325 reduction of *ppw-1* in this strain promotes germline RNAi (Figure 3D). Like DL238, QX1211
326 lacks the *pha-1* antidote (*Ben-David et al., 2017*). Here, the heterozygote genotypes on the
327 negative control and the wild-type heterozygote on *par-1* showed embryonic lethality arising
328 from the incompatibility.
329
330 (iv) Strains CB4852, KR314, and ECA369 exhibited *ppw-1*-independent rescue, in which the
331 two heterozygote genotypes exhibited levels of embryonic lethality that were equivalent to each
332 other and significantly higher than the wild isolate on its own. This suggests that N2 alleles other
333 than *ppw-1* promote the RNAi response in these genetic backgrounds (Figure 3E).
334
335 **RNAi against GFP confirms strain-specific variation**
336
337 Wild isolates exhibit heritable variation in embryonic pathways, as evidenced by differences in
338 lethality following single-gene perturbations; these mutations may confound our ability to
339 measure RNAi using those targets (*Paaby et al., 2015*). To verify that the responses we measured
340 here were due to deficiencies in germline RNAi, and not to differences in developmental
341 pathway function (e.g. for *par-1*), we introgressed a germline-expressed GFP construct
342 (*stIs10024*, in which GFP fused to histone H2B is driven by *pie-1*) into four of our low-response
343 strains and measured fluorescence following RNAi against GFP. The strains represented the four
344 distinct RNAi response patterns observed in the *ppw-1* complementation tests (Figure 3).
345
346 As expected, strains CB4856, QX1211 and JU1522 showed negligible RNAi response in young
347 hermaphrodite germlines, with no initial difference in GFP fluorescence intensity between

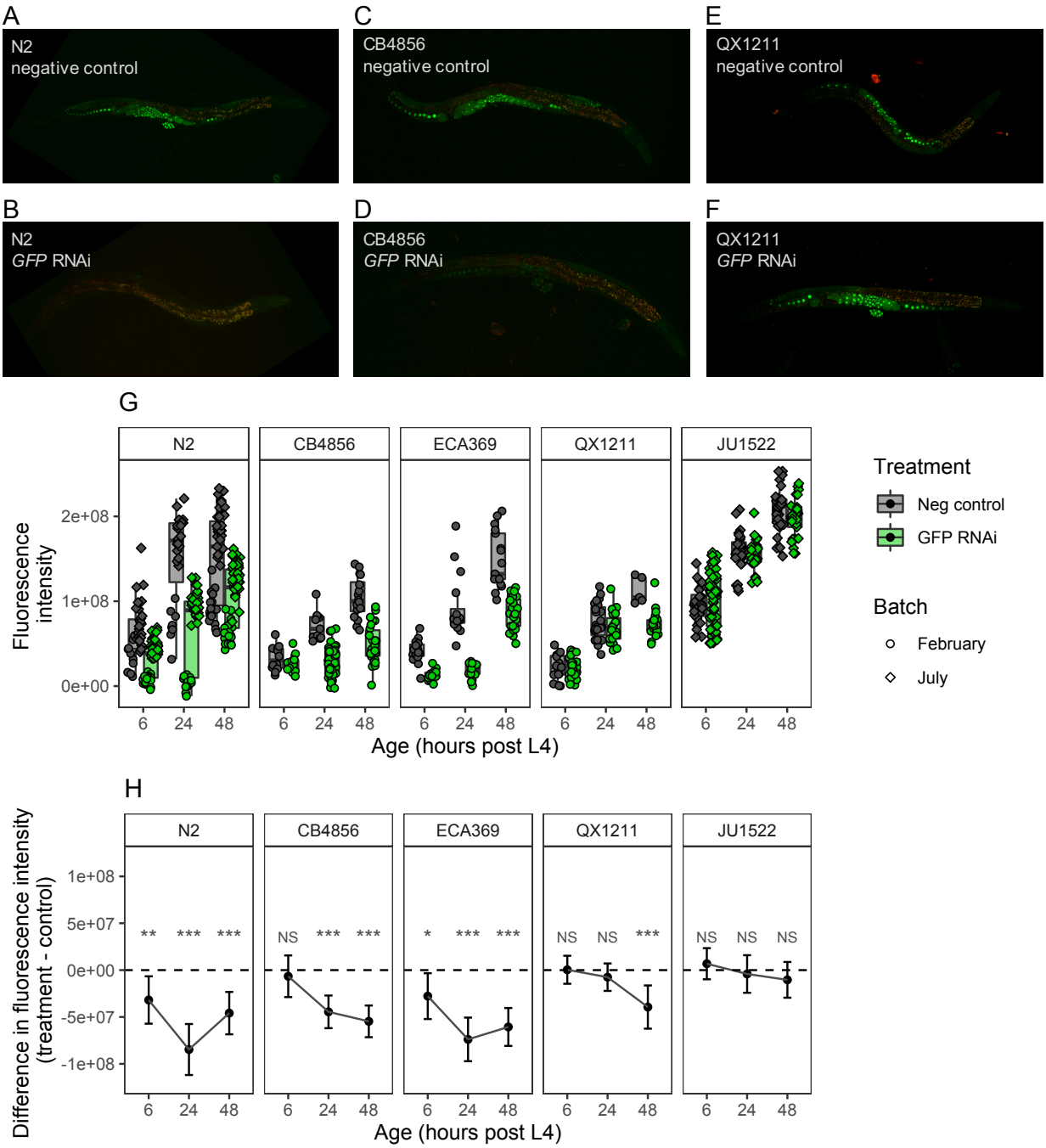

Figure 4. RNAi against germline-expressed GFP in wild-type strains. (A) - (F) Representative images of control and treated worms, all at 24hrs post L4 stage, are shown for N2, CB4856 and QX121. Green indicates GFP fluorescence; the red channel is overlaid on these images to show autofluorescence. (G) Whole-worm fluorescence intensity for worms imaged at 6, 24, and 48hrs post L4 stage; each point represents fluorescence measured for a single individual. (H) The difference in fluorescence intensity between treated and untreated samples; error bars represent standard error. Significance levels (Tukey's contrasts): $p<0.001$ (***), $p<0.01$ (**), $p<0.05$ (*).

357 treated and untreated worms (Figure 4). Also consistent with measurements of RNAi using *par-*
358 *1*, CB4856 showed diminished fluorescence in older hermaphrodites, confirming a delayed
359 response, and JU1522 showed no evidence of RNAi. Overall, QX1211 exhibited a very weak
360 RNAi response, though we did not observe any on/off variation in fluorescence across individual
361 worms. Strain ECA369, however, showed a significant reduction in GFP fluorescence even at
362 the earliest timepoint, suggesting that apparent resistance to *par-1* RNAi may be mediated by
363 alleles modifying PAR-1 function rather than germline RNAi.
364
365 **Genetic complementation between wild isolates implicates diverse and polygenic basis for**
366 **germline RNAi incompetence**
367
368 To examine whether the alleles that limit germline RNAi are unique or shared across wild
369 isolates, we performed complementation tests by crossing low-response strains to each other. As
370 above, we measured embryonic lethality following *par-1* RNAi exposure in the F1 generation.
371 We performed a total of six tests, with each pairwise cross for strains CB4856, DL238, KR314
372 and QX1211 (Figure 5). We chose these strains based on their apparent diversity in PPW-1
373 function (Figure 3) and compatibility at the *zeel-1*;*peel-1* locus (*Andersen et al., 2012*).
374
375 The CB4856 × QX1211 heterozygote produced significantly more dead embryos, indicating an
376 increased RNAi response, than either strain on its own (Figure 4A). This implies that alleles that
377 dampen the RNAi response are not shared between these two strains, as their function is at least
378 partially rescued by the alternate genetic background. Given that CB4856 and QX1211 exhibit
379 responses that are dependent on *ppw-1* but opposite to each other (Figure 3), their
380 complementation may be occurring at *ppw-1* itself.
381
382 DL238 had exhibited a *ppw-1*-dependent response (Figure 3), suggesting that, like CB4856, it
383 may be deficient in PPW-1 activity. However, CB4856 × DL238 hermaphrodites also showed a
384 rescued RNAi response (Figure 5B), again implicating distinct mechanisms in these strains.
385 Interestingly, we observed that the direction of the CB4856 × DL238 cross affected the
386 magnitude of the RNAi rescue. For all pairwise crosses, we performed matings in both directions
387 except those with KR314, as males in this strain are infertile (*Hodgkin & Doniach, 1997*). The
388 direction of the cross had no effect, except for CB4856 × DL238, in which heterozygotes sired

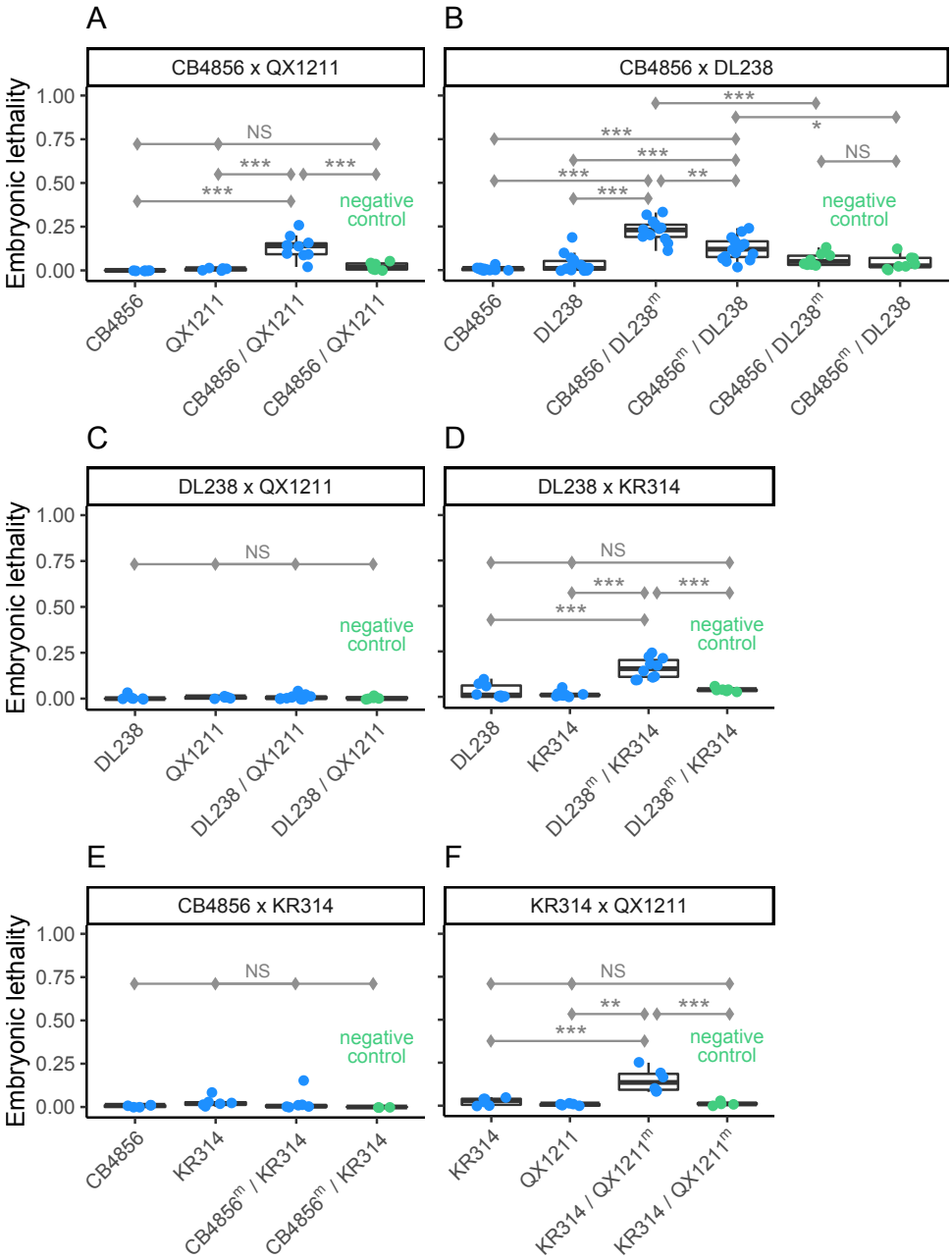

Figure 5. Pairwise complementation tests between four wild isolates with low RNAi response. (A) - (F) Response was measured by embryonic lethality following RNAi by feeding against the embryonic target *par-1*. The heterozygote genotypes were generated by crossing males and hermaphrodites in both directions (A) - (C), except for crosses with strain KR314, which does not produce fertile males (D) - (F). With the exception of CB4856 × DL238 (B), in which hermaphrodites sired by DL238 exhibited a significantly stronger response than those sired by CB4856, cross direction had no effect on embryonic lethality in the next generation and plots show pooled data. Significance levels (Tukey's contrasts): $p<0.001$ (***), $p<0.01$ (**), $p<0.05$ (*).

399 by DL238 exhibited a stronger response than those sired by CB4856 (Figure 5B). This bias is not
400 observed in the negative control and is not explained by a *pha-1;sup-35* incompatibility between
401 CB4856 and DL238, which is not expected to drive F2 lethality (*Ben-David et al., 2017*).
402
403 DL238 failed to complement QX1211 (Figure 5C), but did complement KR314 (Figure 5D),
404 indicating shared and distinct mechanisms, respectively. These outcomes for DL238 are the
405 opposite of those observed for CB4856 crossed to the same strains (Figure 5A, 5E), reinforcing
406 the conclusion that CB4856 and DL238 harbor distinct genetic mechanisms for weak germline
407 RNAi, despite similar responses under *ppw-1* manipulation (Figure 3). Further evidence for
408 distinct genetic mechanisms is seen in the complementation of KR314 × QX1211 (Figure 5F).
409
410 These observations of complementation between wild strains indicate that natural populations
411 harbor unique alleles mediating germline RNAi, and that variation in RNAi response is
412 polygenic. Coupled with the results of the *ppw-1* complementation tests (Figure 3), which
413 suggest that weak RNAi is multigenic within strains, we conclude that variation in germline
414 RNAi is a highly complex trait.
415
416 **Patterns of gene expression implicate differential regulation of RNAi factors**
417
418 To evaluate whether additional causal factors for weak germline RNAi include known RNAi
419 genes, including other Argonautes, we examined expression variation at 62 loci (listed in Table
420 1). We performed RNA-seq on low-response strains CB4856 and QX1211, on responsive strains
421 N2 and JU1088, and on strain EG4348, which shows an intermediate response (*Paaby et al.,*
422 *2015*). RNA samples were prepared from young, reproductively mature hermaphrodites reared on
423 *par-1* RNAi, *pos-1* RNAi, and the empty feeding vector as a negative control.
424
425 For each gene, we looked for evidence of differential expression between each wild isolate and
426 N2 without inducing RNAi (the control condition), or between *par-1* or *pos-1* RNAi and the
427 control within each strain. In both analyses, we observed significant differences in relative
428 expression at multiple genes, in both directions. In other words, the directionality of expression
429 was not associated with a putatively active RNAi response (Figure 6A-B).
430

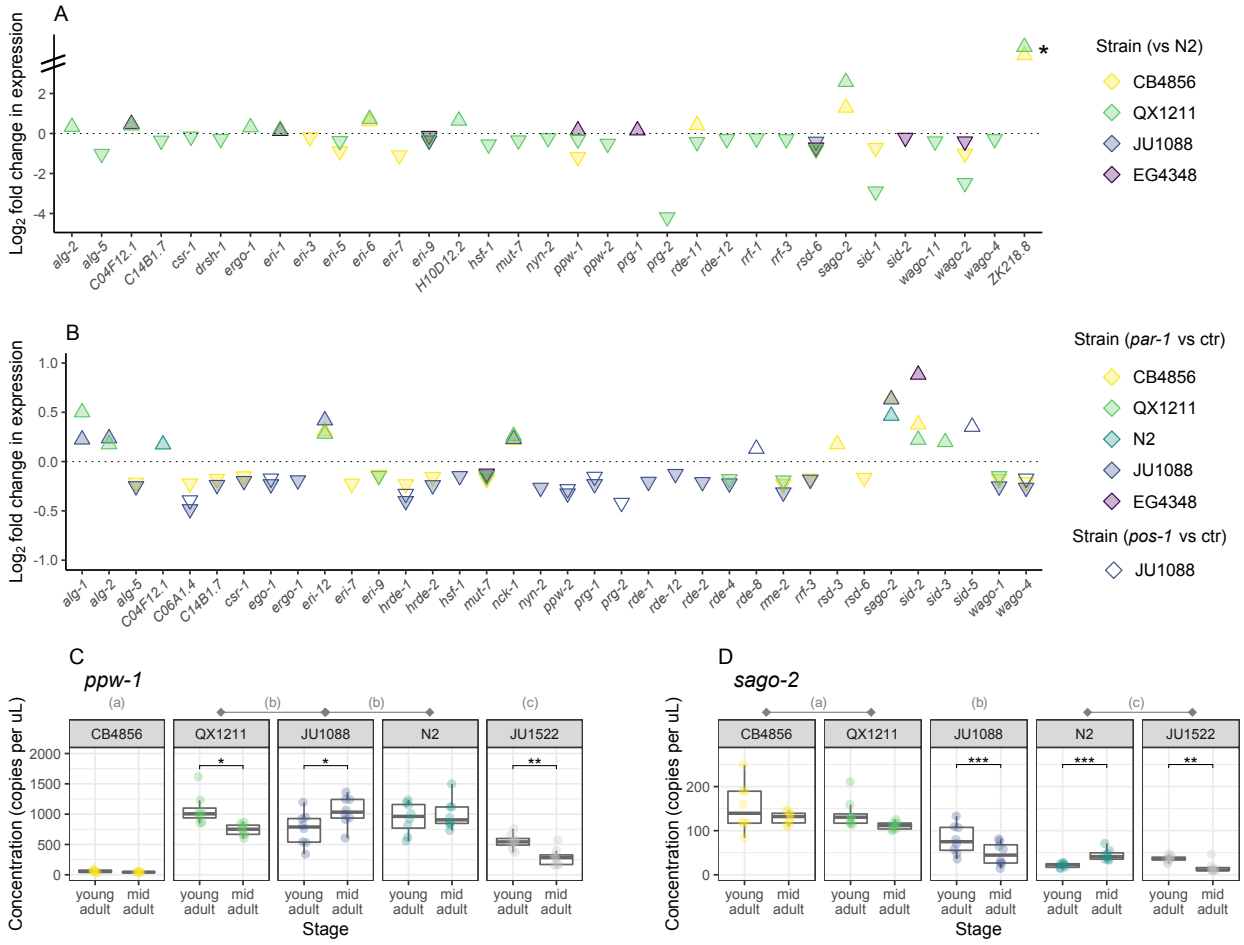

Figure 6. Differential gene expression for RNAi factors across strain and RNAi conditions. (A) - (B) We examined 62 genes for differential expression via RNA-seq; only those with significant results (FDR<0.1) are displayed. (A) Up or down arrows indicate differential expression between N2 and low-response strains CB4856 and QX1211, moderately responsive strain EG4348, and high-response strain JU1088, tested without induction of RNAi. The (*) at *ZK218.8* indicates differential expression beyond the y-axis scale; this gene is not expressed in the N2 reference strain and has been classified as a pseudogene. (B) Arrows indicate differential expression within each strain, between the control condition (no RNAi) and RNAi against *par-1* and *pos-1*. (C) - (D) Expression differences via droplet digital PCR for *ppw-1* and *sago-2*. Ten strains were evaluated (Figure S4); a subset are shown here. Across strains, significant differences (Tukey's contrasts, p<0.05) are indicated by letter groupings; for example, QX1211, JU1088, and N2 have equivalent concentrations of *ppw-1*, while CB4856 and JU1522 concentrations are significantly different from all others. Within each strain, significant differences between developmental stages (pairwise contrasts with Bonferroni correction) are indicated by: p<0.001 (***), p<0.01 (**), p<0.05 (*).

447 Relative to N2, strains with weakest germline RNAi exhibited the greatest degree of differential
448 expression. That is: QX1211, then CB4856 showed the most differences across the gene set; the
449 moderately responsive strain EG4348 showed a handful of modest differences; and the strongly
450 responsive strain JU1088 showed a modest difference in expression for only one gene (Figure
451 6A). Of the genes differentially expressed (FDR<0.1) by both CB4856 and QX1211, the
452 direction of expression was concordant but for one exception (*rde-11*). Notable include a strong
453 reduction in expression by QX1211 at *prg-2*; reduction by both QX1211 and CB4856 at *eri-5*,
454 *ppw-1*, *sid-1*, and *wago-2*; and increased expression by both strains at *sago-2* and *ZK218.8*. The
455 unnamed gene *ZK218.8*, previously identified as a potential Argonaute (*Yigit, 2007*), is classified
456 as a pseudogene and remains unexplored in the literature. We observed no expression of
457 *ZK218.8* in N2, JU1088 or EG4348, but it is actively transcribed in CB4856 and QX1211,
458 suggesting pseudogenization may have occurred in some strain lineages but not in others.
459
460 Relative to N2, strains with the greatest degree of differential expression were also the most
461 genetically diverged. However, RNAi incompetence does not appear to be a function of genetic
462 distance from the reference strain. Highly diverged isolates ECA701, JU561, and XZ1516
463 (*Crombie et al., 2019*) were responsive to *par-1* RNAi (data not shown), and RNAi sensitivity for
464 55 wild isolates in (*Paaby et al., 2015*) showed no relationship with divergence from N2 (Figure
465 S3).
466
467 Within each strain, we observed more instances of differential expression in the *par-1* vs control
468 comparison than in the *pos-1* comparison. Only JU1088, which exhibits the strongest germline
469 RNAi response of these five strains (*Paaby et al., 2015*), showed significant differences on *pos-1*,
470 all of which were in the same direction as the *par-1* responses (Figure 6B). All of the genes that
471 were differentially expressed (FDR<0.1) for multiple strains showed consistent directionality as
472 well. None of the strains exhibited differential expression at *ppw-1*, but CB4856, N2, and
473 JU1088 showed strong up-regulation of *sago-2* on *par-1* RNAi.
474
475 The WAGO Argonautes *ppw-1* and *sago-2*, which reside ~17cM apart on chromosome I, share
476 high sequence identity. In some strains, including QX1211, poor mapping of short reads to the
477 reference genome (*Cook et al., 2017*) suggests instances of gene divergence or duplication. We
478 resolved sequence ambiguities via de novo assembly of paired-end reads and long read

479 sequencing, and observed that QX1211 carries *ppw-1*-like alleles at both loci (File S1). To
480 validate our RNA-seq observations of *ppw-1* and *sago-2* expression, and to evaluate additional
481 strains, we designed a droplet digital PCR (ddPCR) experiment to measure both transcripts
482 simultaneously and discriminate between them using transcript-specific labels. We tested all
483 strains thus far discussed: the seven low-response strains for which we tested *ppw-1* function
484 (Figure 3), as well as responsive strains N2 and JU1088 and moderately responsive strain
485 EG4348. We measured native expression; worms were not treated with RNAi. To evaluate
486 whether *ppw-1* or *sago-2* expression changed as worms aged, we also collected RNA from two
487 developmental timepoints, young adult and mid adult.
488
489 Consistent with the RNA-seq results, CB4586 exhibited very low *ppw-1* expression (Figure 6C,
490 Figure S4), and CB4856 and QX1211 exhibited high *sago-2* expression (Figure 6D, Figure S4).
491 Overall, *ppw-1* expression was about an order of magnitude higher than that of *sago-2*, and the
492 expression levels of both genes differed significantly across strains (Table S1). Changes in
493 expression between developmental timepoints also differed significantly across strains, for both
494 genes (Figure 6C-D).
495
496 Expression levels of *ppw-1* and *sago-2* showed no clear correlation with RNAi responsiveness.
497 Across all ten strains, the combined expression of *ppw-1* and *sago-2* was both highest and lowest
498 in two strongly resistant strains: QX1211 and JU1522, respectively (Figure 6C-D). We have
499 consistently observed negligible germline RNAi in JU1522, including no rescue when crossed
500 with N2 (Figure 3), and no response even at later age (Figure 4); this strain exhibits the weakest
501 response we have observed. One possibility is that both high and low expression of *ppw-1* and
502 *sago-2* can limit germline RNAi. This hypothesis is consistent with our observation that a
503 haploid dose of *ppw-1* increases the RNAi response in QX1211 (Figure 3D), and with the prior
504 finding that *ppw-1* and *sago-2* encode functionally interchangeable proteins that can compensate
505 each other (*Yigit et al., 2006*), but not with the observation that overexpression these factors
506 increases RNAi sensitivity in N2 (*Yigit et al., 2006*). N2 and JU1088, the two strains with the most
507 robust germline RNAi response in our analysis, exhibit intermediate baseline levels of *ppw-1* and
508 *sago-2* combined (Figure S4), and both exhibit significant up-regulation of *sago-2* on *par-1*
509 RNAi (Figure 6B). Notably, so does CB4856; it shows the highest baseline level of *sago-2*
510 (Figure S4), and over time increases *sago-2* expression at a higher rate than N2 (Figure 6B). This

511 may explain why CB4856, which carries a putatively deficient *ppw-1* allele (*Tijsterman et al.,*
512 *2002*), is able to mount a delayed germline RNAi response while the N2 *ppw-1* null mutant is not
513 (Figure 1B).
514
515 ***C. elegans* RNAi genes show lineage-specific diversification and pseudogenization**
516
517 To identify candidate genes for the weak RNAi responses we observed, we examined genotypes
518 at known RNAi genes (listed in Table 1) among the seven low-response strains. Of 62 genes,
519 five harbored at least one instance of a high impact mutation predicted to disrupt the encoded
520 protein. Occurrences were mostly strain-specific: in addition to the frameshift mutation at *ppw-1*
521 in CB4856 (*Tijsterman et al., 2002*), we observed high impact variants at *ergo-1* in ECA369, at
522 *sago-2* in DL238, at *lin-15b* in QX1211, and at *eri-7* in CB4856, DL238 and ECA369 (Table
523 S2). Given that the mutation at *ppw-1* does not fully explain weak germline RNAi in CB4856
524 (*Tijsterman et al., 2002*) and that additional causal factors appear to be linked nearby (Figure 1B,
525 (*Pollard & Rockman, 2013*), we propose *eri-7*, which is 0.34cM from *ppw-1*, as a candidate; in
526 addition to the high impact mutation, which putatively affects splicing, CB4856 exhibits reduced
527 *eri-7* expression (Figure 6).
528
529 We also observed alleles that were diverged from the N2 reference genotype but did not carry
530 disruptive high impact variants, suggesting that selection has driven potentially divergent gene
531 function. We classified such "functional diverged alleles" as those with at least five amino acid
532 substitutions, at least 1% divergence across sites, and no high impact mutations. QX1211
533 harbored 14 functional diverged alleles (Table S2), a subset of which are also differentially
534 expressed: *eri-1*, *eri-6*, *eri-9*, *nyn-2* and *rde-12* (Figure 6). Notably, we observed elevated
535 variation at *hsf-1*. This transcription factor is a master regulator of many RNAi genes, and HSF-1
536 activity explains stochastic differences in heritable RNAi responses among individuals with an
537 isogenic N2 background (*Houri-Zeevi et al., 2020*). Two of the seven strains carry functional
538 diverged alleles at *hsf-1*, and another four show poor read mapping, suggesting further allelic
539 divergence (Table S2). Relative to N2, *hsf-1* expression is reduced in QX1211 (Figure 6).
540
541 To better characterize patterns of molecular diversity at RNAi genes, we expanded our 62-gene
542 analysis to the population level by querying 403 strain isotypes in CeNDR (*Cook et al., 2017*).

543 **Table 1.** Molecular diversity at 62 RNAi genes, from 403 strain isotypes. "Functional diverged alleles"
544 are those with at least 1% nucleotide divergence from the reference genome, including at least five
545 moderate mutations, such as amino acid substitutions, and no disruptive high impact mutations, such as
546 frameshifts or stop-gains. "Pseudogenized alleles" are those with at least one high impact mutation called
547 with high confidence and at which 1% or more of the sites are diverged or missing, or those with at least
548 50% of the sites with missing calls. Potential pseudogenization was assessed with respect to the reference
549 genome and considered even for those Argonautes already classified as putative pseudogenes on
550 Wormbase.
551

Class	Gene	Nucleotide diversity (π)	No. strains with functional diverged alleles	No. strains with pseudo-genized alleles
Argonaute (AGO)	*alg-1*	7.20E-04	0	0
	alg-2	8.53E-04	0	19
	alg-3	6.86E-04	0	1
	alg-4	6.08E-04	10	5
	alg-5	3.75E-04	0	0
	rde-1	4.98E-04	2	0
Argonaute (PIWI)	*ergo-1*	1.18E-03	0	8
	prg-1	1.77E-03	0	0
Argonaute (WAGO)	*C04F12.1*	2.50E-04	0	34
	csr-1	6.59E-04	0	0
	hrde-1	1.84E-04	4	3
	nrde-3	3.39E-04	22	0
	ppw-1	2.77E-04	0	2
	ppw-2	5.35E-04	0	0
	sago-1	1.23E-03	0	4
	sago-2	1.26E-03	1	25
	wago-1	9.37E-04	0	0
	wago-10	9.64E-06	58	2
	wago-4	7.70E-06	0	0
	wago-5	9.17E-06	0	48
	C06A1.4	1.07E-03	0	0
Argonaute (pseudo)	*C14B1.7*	6.47E-04	0	0
	H10D12.2	3.00E-04	0	25
	prg-2	6.59E-04	0	3
	wago-11	7.58E-05	0	64
	wago-2	7.78E-04	0	0
	ZK218.8	4.08E-04	0	11
	dcr-1	6.37E-04	49	0
Other RNAi factor	*drh-1*	2.35E-04	40	0
	drsh-1	1.11E-03	0	0
	ego-1	1.07E-04	0	0
Other RNAi factor	*eri-1*	2.37E-04	23	0
	eri-12	5.00E-04	23	0
	eri-3	4.37E-04	9	0
	eri-5	7.15E-04	0	1
	eri-6	6.04E-04	36	20
	eri-7	1.74E-04	0	12
	eri-9	7.00E-04	26	0
	hrde-2	9.92E-04	0	0
	hsf-1	5.54E-03	119	0
	lin-15b	2.61E-04	9	53
	mut-7	8.90E-04	0	0
	nck-1	5.01E-04	0	0
	nhl-2	2.22E-04	0	0
	nyn-2	4.47E-04	2	1
	rde-10	1.00E-03	21	1
	rde-11	5.45E-05	0	1
	rde-12	2.46E-03	54	0
	rde-2	1.48E-04	0	0
	rde-4	7.21E-04	0	0
	rde-8	5.03E-06	0	0
	rme-2	2.09E-04	0	0
	rrf-1	1.09E-03	9	0
	rrf-3	1.19E-03	14	0
	rsd-2	2.67E-03	151	4
	rsd-3	2.00E-04	35	0
	rsd-6	2.68E-04	28	0
	sid-1	9.03E-04	0	1
	sid-2	1.44E-03	54	3
	sid-3	2.09E-04	56	1
	sid-5	1.23E-03	0	0
	tofu-5	6.59E-04	0	0

552

553 Estimates of nucleotide diversity (π) per gene were generally high (Table 1) relative to genome-
554 wide averages (*Lee et al., 2021*), with π>0.001 for 14/62 genes (13/55 genes not characterized as
555 pseudogenes). Elevated variation was often, but not always, associated with high-impact
556 mutations in one or more strains (Figure S5). Therefore, to distinguish between instances of
557 pseudogenization and gene loss versus allelic diversification arising from directional or
558 balancing selection acting on functional sequences, we classified alleles as possible pseudogenes

559 if they harbored at least one high impact mutation called with high confidence and if at least 1%
560 of the sites were diverged or missing relative to the reference genome, or if over 50% of sites
561 were missed calls; we classified alleles as functionally diverged as defined above.
562
563 Given the expansion and diversification of Argonautes in nematodes (*Buck & Blaxter, 2013*), we
564 hypothesized that the WAGO genes might be relatively unconstrained and therefore especially
565 susceptible to pseudogenization. Indeed, we saw multiple instances of putative gene loss in one
566 or more strains at WAGOs, but we also saw putative loss across all classifications, including the
567 PIWIs, AGOs, and other RNAi factors (Table 1). Excluding seven genes classified as
568 pseudogenes on Wormbase (*Harris et al., 2020*), 40% (22/55) of the RNAi genes indicated
569 pseudogenization in one or more strains (Table 1). Consistent with active transcription of
570 putative pseudogene *ZK218.8* in some non-reference strains (Figure 6A), we conclude that RNAi
571 genes exhibit an unusually high level of lineage-specific gene loss in *C. elegans*.
572
573 Across the population, we found that 25 genes harbor functional diverged alleles (Table 1).
574 These alleles most often occurred in multiple strains, unlike the pseudogenized alleles, which
575 often occurred singly. A comprehensive analysis is beyond the scope of this paper, but these
576 results are consistent with positive selection driving or maintaining divergent gene function. For
577 example, at *hsf-1* we observed very high polymorphism, including amino acid changes at
578 intermediate frequencies, but no instances of disruptive high-impact mutations (Figure 7A). (We
579 also observed poor read mapping across the locus, which indicates further divergence but may
580 also obscure deleterious mutations.) The apparent absence of loss-of-function alleles at *hsf-1*
581 suggests purifying selection, and its diversification suggests evolutionary lability, potentially as a
582 keystone regulator of small RNA pathways (*Houri-Zeevi et al., 2020*). At other genes, high
583 polymorphism may have accumulated under relaxed selection. The PIWI Argonaute *ergo-1*, for
584 example, exhibits lineage-specific pseudogenization (Figure 7B). Although some of the RNAi
585 genes are near invariant (Figure 7C, Figure S5), the overall level of very high allelic divergence
586 at Argonautes and other known RNAi factors indicates that RNAi pathways are likely evolving
587 dynamically within the *C. elegans* population. These findings suggest that variation at known
588 RNAi genes likely contributes to the observed variability in RNAi response, and that functional
589 characterizations of these genes, which have been universally achieved in N2, may be strain
590 specific.

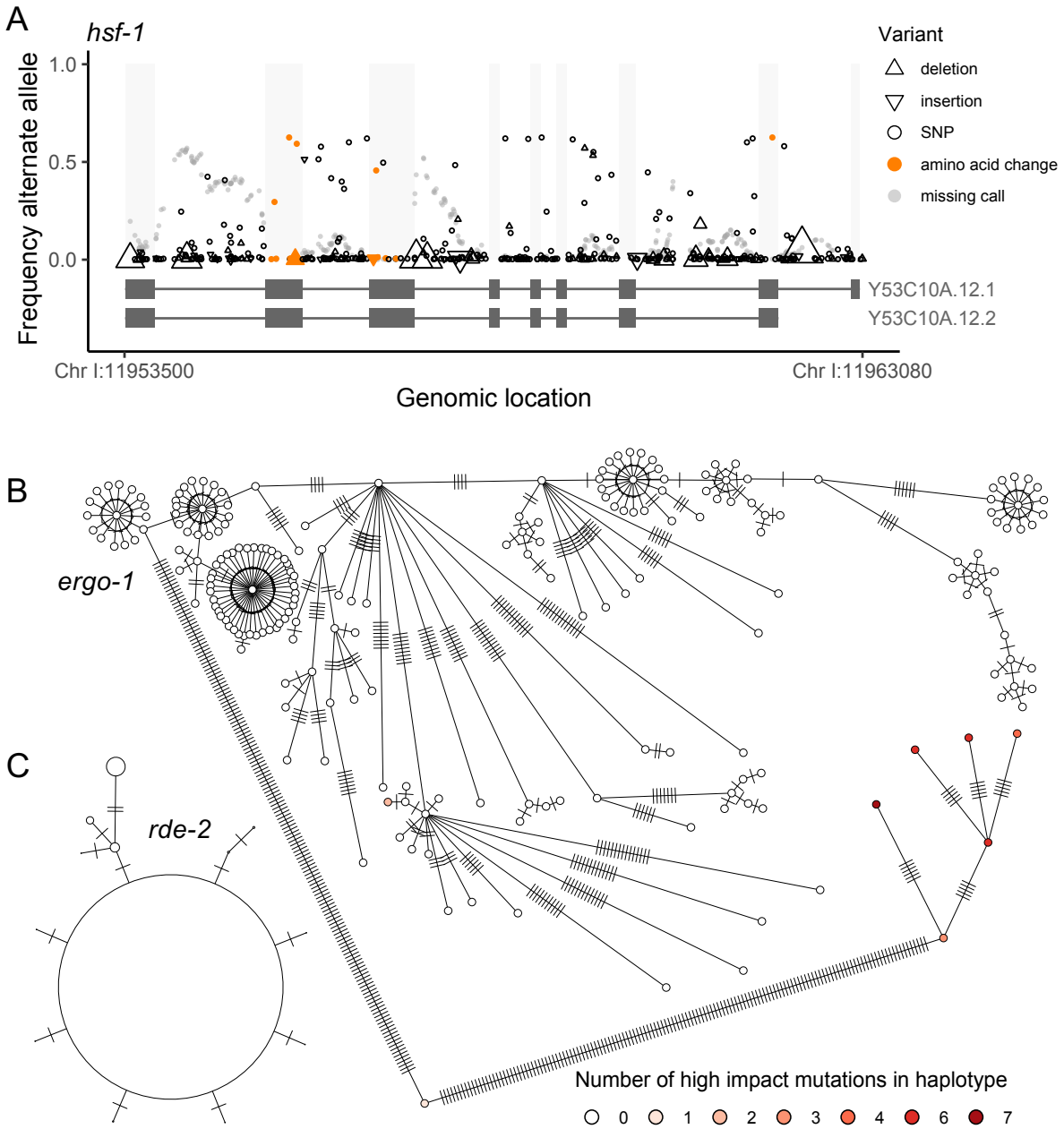

Figure 7. Population-level allelic diversity in RNAi genes across 403 strains. (A) The transcription factor *hsf*-1 shows elevated polymorphism indicative of functional divergence, including: multiple changes to the amino acid sequence, mutations segregating at intermediate frequency, and no observed high impact mutations that disrupt the protein. Each observed mutation is represented as a single point; the up- and down-triangles representing indels are scaled by indel length (range = 1-99, mean = 6.8). (B) The Argonaute *ergo-1* also exhibits elevated polymorphism, but accumulation of high impact mutations in some alleles suggests gene loss by pseudogenization. In this haplotype network, each circle represents a unique haplotype (of one or more strains) and hatch marks indicate mutations. (C) In contrast, *rde-2* exhibits conservation. Most strains belong to the common haplotype; haplotype circles are scaled by frequency.

602 **DISCUSSION**

603

604 In this study, we demonstrate that the failure of some wild-type *C. elegans* strains to mount a
605 robust germline RNAi response occurs by a diversity of mechanisms. Rather than identifying one
606 or more common, shared factors that explain RNAi incompetence, our results indicate that RNAi
607 fails for different reasons in different strains and that the same genes can produce opposite
608 responses. Coupled with high levels of divergence and lineage-specific pseudogenization at
609 known RNAi genes, these findings reposition our understanding of RNAi pathways and
610 processes.

611

612 Sydney Brenner's selection of *C. elegans* as a model species, and N2 as the strain of study, was
613 fortuitous for the future discovery of RNAi (*Félix, 2008*). This system remains the most fertile
614 area for elucidating gene regulation by small RNAs (*Youngman & Claycomb, 2014*), but our
615 understanding is incomplete without incorporating how RNAi phenomena vary at the population
616 level. The N2 reference genome is both independent of (for purposes of experimental control)
617 and inextricably linked to (via evolution) the genomes of other *C. elegans* strains. Thus, RNAi
618 genes and the interactions between them reside in an expanded context, shaped by the
619 evolutionary history of the population. Our finding that germline RNAi incompetence is highly
620 strain-specific offers direct access into identifying conserved and labile components of RNAi
621 pathways. For example, the apparent dispensability of some Argonautes for target cleavage, or
622 gene silencing generally (*Billi et al., 2014*), is probably best understood in the context of a pool of
623 interchangeable factors (*Yigit et al., 2006*), which our data on *ppw-1* and *sago-2* support.

624

625 We show that many RNAi genes have been pseudogenized along specific lineages within the
626 population (Table 1). However, evidence of directional or diversifying selection along other
627 lineages, and at other genes (Table 1), suggests that intraspecific differences in germline RNAi
628 incompetence have not evolved by a straightforward accumulation of loss-of-function variants.
629 Instead, we conclude that RNAi pathways are evolving dynamically in the contemporaneous
630 population. A more complete sequence analysis, on wild-type genomes without ambiguities at
631 unmapped loci, will be valuable in refining microevolutionary dynamics in RNAi pathways and
632 identifying testable hypotheses with respect to allele function and interaction. For example, the

633 non-additivity we observed for *ppw-1* (Figure 3) indicates strain-specific differences that may
634 well occur for other Argonautes, and which will be best interpreted in aggregate.
635
636 The variation in *ppw-1* phenotypes and diversification of other RNAi factors (Figure 3, Table 1)
637 indicate that the activity of RNAi genes is highly context-dependent. Background effects have
638 always plagued genetic analysis (*Chandler et al., 2013*), but the retention of hyperdiverse regions
639 across the *C. elegans* genome (*Lee et al., 2021*), the potential for strong epistasis in the species
640 (*Campbell et al., 2018*), and high evolvability of RNAi (*Nuez & Félix, 2012*) suggest that this
641 system is especially susceptible to functional variability. As such, genetic analysis of RNAi
642 phenotypes in non-reference strains has the potential to yield orthogonal insights into RNAi
643 biology and complement our existing body of knowledge derived from experiments in the lab
644 strain N2 (*Chandler et al., 2013*).
645
646 Given the essentiality of RNAi to numerous biological processes—and the centrality of *C.*
647 *elegans* in RNAi research—is the variation in this system surprising? Perhaps not: the variation
648 we describe here mirrors patterns of RNAi incompetence observed over longer evolutionary
649 timescales. The ability to silence genes by dsRNA appears intermittently, and shows evidence of
650 rapid evolution within the *Caenorhabditis* genus (*Nuez & Félix, 2012; Winston et al., 2007*), across
651 nematodes generally (*Buck & Blaxter, 2013; Dalzell et al., 2011*), and in other systems (*Obbard et*
652 *al., 2009*). Argonautes and associated RNAi factors also exhibit taxon-specific patterns of gene
653 duplication, loss, and diversification, likely representative of diversification of biological
654 functions (*Buck & Blaxter, 2013; Dalzell et al., 2011; Obbard et al., 2009*). RNAi exhibits great
655 lability over long timescales (*Nuez & Félix, 2012*), which we now observe over very short
656 timescales as well.
657
658 The variability we observe suggests that RNAi experiments in the lab do not necessarily target
659 the phenomena most relevant to the animal itself. Exogenous RNAi likely induces responses that
660 evolved for antiviral immunity, but our understanding of nematode immunity is still young (*Ashe*
661 *et al., 2013, 2015; Félix et al., 2011; Sarkies et al., 2013; Wilkins et al., 2005; Yigit et al., 2006*). Orsay
662 virus, the only natural-occurring virus known to infect *C. elegans*, invades intestinal cells and is
663 horizontally, but not vertically, transmitted (*Félix et al., 2011; Franz et al., 2014*). However,
664 vertically transmissible viral-like RNAs have been detected in the germlines of wild-caught

665 *Caenorhabditis* isolates (*Richaud et al., 2019*), suggesting undiscovered host-pathogen dynamics.
666 The piRNA pathway is active in the germline and presumed critical for maintaining genome
667 integrity (*Wilson & Doudna, 2013; Youngman & Claycomb, 2014*). We found that germline RNAi
668 increases in strain QX1211 after consecutive generations at ≥18°C (unpublished data), which we
669 hypothesize may be associated with changes in piRNA-like pools of small RNAs that co-occur
670 with onset of the mortal germline phenotype (*Frézal et al., 2018*). One possibility is that
671 competition between exogenous and endogenous RNAi forces induction of one pathway over the
672 other (*Yigit et al., 2006; Youngman & Claycomb, 2014*), which may explain the stochasticity in
673 QX1211 phenotypes. Since *ergo-1* laboratory mutants show enhanced exo-RNAi but reduced
674 endo-RNAi (*Yigit et al., 2006*), this gene, which exhibits extreme allelic diversification in nature
675 (Table 1, Figure 6), may gatekeep RNAi pathway activity differently in different isolates.
676 Another possibility is that in the wild, RNAi in the germline matters most to future generations.
677 Strains resistant to RNAi upon exposure can show transgenerational sensitivity (*Tijsterman et al.,*
678 *2002*), and a growing body of research emphasizes the outsized role of RNAi in transgenerational
679 inheritance (*Houri-Zeevi et al., 2020, 2021*). Thus, germline RNAi incompetence as we observe it
680 in the lab may only be part of the story in nature.
681
682 RNAi is a complex and intricate collection of phenomena. RNAi responses are sensitive to
683 environmental conditions (*Houri-Zeevi et al., 2021*) and susceptible to unexpected outcomes (*De-*
684 *Souza et al., 2019*), which in turn could be mediated differently in different genetic backgrounds.
685 Much of our effort here went to developing protocols that could discriminate between distinct
686 RNAi responses in wild-type strains while avoiding confounding effects. For example, to prevent
687 native differences in developmental timing or gene expression from confounding RNAi
688 phenotypes (*Shiu & Hunter, 2017*), we exposed the parental generation to dsRNA as unfed L1
689 larvae instead of as L4s (*Kamath et al., 2001*). However, the extent of condition-dependent
690 interactions in RNAi may preclude true experimental control. For example, temperature likely
691 plays an unseen hand in RNAi experimentation, given the exquisite sensitivity of *C. elegans* to
692 temperature (*Testa et al., 2020*) and the intimate relationship between temperature and other
693 stresses and RNAi (*Frézal et al., 2018; Houri-Zeevi et al., 2021; Pagliuso et al., 2021*). We controlled
694 environmental temperature by conducting all RNAi assays at 20°C, but RNAi competence may
695 be maximized at different temperatures in different strains. On the other hand, temperature may
696 be used to uncover plastic and adaptive responses (*Paaby & Testa, 2018*). In this system, which

697 increasingly appears to be dominated by transgenerationally inherited small RNA programs
698 (*Houri-Zeevi et al., 2021*), temperature may prove a valuable tool in exposing the variability and
699 function of *C. elegan*s inheritance systems in the wild (*Frézal et al., 2018*).
700
701 **MATERIALS AND METHODS**
702
703 **Strains used in this study**
704
705 Table S3 contains a complete list of strains used in this study. To introduce germline-expressed
706 GFP into wild isolates, we introgressed *zuIs178 [his-72(1kb 5' UTR)::his-*
707 *72::SRPVAT::GFP::his-72 (1KB 3' UTR) + 5.7 kb XbaI - HindIII unc-119(+)]; stIs10024 [pie-*
708 *1::H2B::GFP::pie-1 3' UTR + unc-119(+)]* into strains CB4856, ECA369, JU1522 and QX1211
709 by crossing to RW10029 and backcrossing to the wild strain for 10-18 generations.
710
711 **Worm husbandry**
712
713 Worms were cultured following standard protocol (*Stiernagle, 2006*), though we added 1.25%
714 agarose to plates used to maintain non-N2 wild isolates, to avoid burrowing. Worms were
715 maintained at 20°C without starving for at least three generations before initiating an experiment,
716 with the exception of QX1211, which was maintained at 18°C to avoid induction of the mortal
717 germline phenotype (*Frézal et al., 2018*).
718
719 **RNA interference**
720
721 *General culture conditions*
722
723 RNAi was induced by feeding and experiments were carried out on plates, at 20°C, based on
724 methods previously described (*Ahringer, 2006; Kamath et al., 2001*). In brief: to target endogenous
725 germline-expressed genes, we fed worms HT115 *E. coli* bacteria that had been transformed with
726 the pL4440-derived *par-1* (H39E23.1), *par-4* (Y59A8B.14), *pos-1* (F52E1.1), or GFP feeding
727 vector (*Timmons et al., 2001*). The *par-1* and *pos-1* vectors were obtained from the Ahringer
728 feeding library (*Kamath & Ahringer, 2003*); *par-4* was a gift from M. Mana. To target GFP, we

729 transformed HT115 with pL4417, which carries 0.7 kb of GFP coding sequence (*Timmons et al.,*
730 *2001*). We used *E. coli* carrying the empty pL4440 vector as a negative control. Bacteria were
731 streaked from frozen stocks onto LB agar plates with carbenicillin (25 ug/mL) and tetracycline
732 (12.5 mg/mL); liquid cultures were inoculated with 5-10 colonies from <1 week old plates, into
733 LB broth with carbenicillin (50 ug/mL) and tetracycline (12.5 mg/mL) and incubated for 16-
734 18hrs shaking at 37°C, then amplified in a 1:200 dilution with carbenicillin (50 ug/mL) for 6hrs.
735 Seeded plates were incubated in the dark at room temperature and used no earlier than 44hrs and
736 no later than 78hrs. Experimental worms were exposed to RNAi bacteria as L1s by hatching on
737 RNAi plates, synchronized either by bleaching (*Stiernagle, 2006*) or by timed egg-laying by the
738 hermaphrodite mothers.
739
740 *Embryonic lethality assays*
741
742 To measure RNAi response by phenotypic penetrance, we targeted *par-1* or *pos-1* transcripts in
743 the hermaphrodite germline and measured embryonic lethality in the next generation.
744 Experimental worms were reared on RNAi plates and transferred as L4s to fresh RNAi plates for
745 the egg-laying assay, remaining continuously exposed to RNAi bacteria since their hatching. For
746 all experiments except those explicitly testing variation in penetrance between individual worms
747 (Figure 1B, Figure 3C), the L4 hermaphrodites were pooled in small groups of 4-6 on 6-10
748 replicate assay plates. For the complementation tests (Figure 3, Figure 4, Figure S2), all embryos
749 within the first ~15hrs of egg-laying were scored for hatching, typically 100-200 embryos per
750 plate. For assays testing RNAi within a defined window of reproductive maturity, we scored the
751 embryos laid in a 4-6hr window within the first 8hrs of egg-laying (Figure 1A), or a 2hr window
752 4hrs after egg-laying began (Figure 2C). For the experiment measuring RNAi in individual
753 worms over their reproductive lifespan (Figure 1B, Figure S1), the L4 hermaphrodites were
754 singled to RNAi plates, permitted to lay embryos, and continually transferred to fresh plates until
755 they ceased to lay, or laid only unfertilized eggs. To score embryos as dead or alive, we removed
756 the egg-laying adult(s), incubated the plates at 20°C for 24hrs, and counted (dead) embryos and
757 hatched larvae using a stereoscope. Experiments included 6-10 (RNAi treatment) or 4-6
758 (negative control) replicate plates.
759

760 To test the effect of genotype on embryonic lethality following exposure to RNAi, the counts of
761 dead embryos and hatched larvae from each replicate plate were bound together as a single
762 response variable and modeled with a generalized linear model with a quasibinomial error
763 structure, implemented by the *glm* function in R. The model included a single linear predictor for
764 genotype and took the form $E(Y)=g^{-1}(\beta_0+\beta_{genotype})$. Within each experiment, differences between
765 specific genotypes were assessed by pairwise contrasts using the "Tukey" specification in the
766 function *glht* in the R package *multcomp* (*Hothorn et al., 2008*).
767
768 *RNAi against GFP*
769
770 To measure germline RNAi by GFP knockdown, worms carrying a histone-linked GFP driven by
771 a *pie-1* promoter were fed RNAi bacteria targeting GFP. Synchronized animals were grown on
772 RNAi plates, then individually selected for imaging at the following stages: young adults (6±2hrs
773 after exiting L4 stage), day one adults (24±2hrs), and day 2 adults (48±2hrs). For whole worm
774 fluorescence imaging, animals were anesthetized with 10mM NaN_3 and mounted on 2% agarose
775 pads, then imaged using a 10× objective with the PerkinElmer UltraVIEW VoX spinning disk
776 confocal microscope equipped with an EM-CCD camera. Raw images were exported as
777 OME.TIFF files. We used Fiji (*Schindelin et al., 2012*) to acquire the sums of intensity in the Z
778 projection, then quantitated the GFP fluorescence by subtracting the integrated intensity of the
779 background, over the area of the worm, from the integrated intensity of the whole animal. To test
780 whether RNAi-treated worms exhibited reduced fluorescence relative to control worms, we
781 analyzed the six samples (three treatment timepoints, three control timepoints) for each strain
782 using a one-way ANOVA, then performed treatment-control contrasts within each timepoint
783 using the R function *TukeyHSD()*.
784
785 **Single-molecule fluorescence *in situ* hybridization**
786
787 *Sample preparation and imaging*
788
789 Custom Stellaris FISH probes were designed with the Stellaris Probe Designer (LGC Biosearch
790 Technologies). We excluded polymorphic sites during probe design. Worms were synchronized
791 on tryptone-free NGM agar plates at the L1 stage and reared on RNAi bacteria as described

792 above. Embryos were extracted by standard bleaching/washing, fixed using 3.7% formaldehyde
793 in RNase-free phosphate buffered saline, and hybridized (100nM at 37°C for 4hrs) with a Quasar
794 570 labeled probe set targeting either *par-1* or *par-4*, following the manufacturer's instructions.
795 Samples were mounted using VECTASHIELD antifade mounting medium with DAPI (Vector
796 Labs #H-1200) on no. 1 cover slides. Images were captured with a 100X oil immersion objective
797 on a PerkinElmer UltraVIEW VoX spinning disk confocal microscope equipped with an EM-
798 CCD camera and piezoelectric motorized stage. Three-dimensional image stacks were collected
799 using Volocity 3D visualization software (PerkinElmer) and exported as TIFF files.
800
801 *Quantitative Analysis*
802
803 We created image segmentation masks and counted chromosome clusters manually using ImageJ
804 (*Schneider et al., 2012*). Single molecule FISH spot quantification was performed using Aro, a
805 MATLAB-based, machine learning pipeline designed for single-molecule visualization in worm
806 embryos (*Wu & Rifkin, 2015*). We used multiple samples from each of the genetic backgrounds
807 and treatments to create the training sets for the random forest classifier. To test whether means
808 or variances in transcript counts differed for RNAi-treated versus untreated samples within a
809 strain, we applied two-sample *t*-tests and *F*-tests, respectively. For these tests, we only
810 considered early stage embryos (up to four cells). To evaluate changes in transcript abundance
811 over a wider range of embryonic development, we considered embryos with up to 30 nuclei and
812 used ANCOVA to ask whether, adjusted for embryo stage, transcript levels varied across strains
813 within the negative control condition; and whether, adjusted for embryo stage, transcript levels
814 varied between control and treatment conditions within a strain. We used minimal model
815 selection to test for changes in the way transcript level depended upon embryo stage (i.e. changes
816 in slope). We estimated ANCOVA effect sizes as ω^2 using the R package *sjstats* (*Lüdecke, 2018*).
817
818 **RNA-seq**
819
820 *Library preparation and sequencing*
821
822 Healthy cultures of strains N2, CB4856, QX1211, JU1088 and EG4348, reared for several
823 generations without starving or bleaching, were bleached to retrieve large numbers of embryos.

824 Synchronized L1 larvae were reared on plates with *par-1*, *pos-1*, or empty RNAi feeding vector,
825 details as described above. Young, reproductively mature hermaphrodites were washed off plates
826 and rinsed twice with M9, then RNA was extracted with TRIzol (Invitrogen #15596026) and
827 RNeasy columns (Qiagen #74104), following (*He, 2011*). All samples were collected and
828 processed simultaneously and in triplicate, starting with replicate plates of worms. cDNA was
829 generated from fresh RNA samples, using 500ng of RNA and 10 cycles of PCR. Libraries were
830 prepared with the NEBNext Ultra II Directional RNA Library Prep Kit for Illumina (NEB
831 #7760) and quality checked using an Agilent 2100 Bioanalyzer. BluePippon (Sage Science) was
832 used to size-select fragments in the pooled library, and sequencing was performed using Illumina
833 NextSeq for single-end 75bp reads. Sequencing was performed by the Molecular Evolution Core
834 facility at the Georgia Institute of Technology.
835
836 *Alignment and gene expression quantification*
837
838 Before alignment, Illumina TruSeq adapters were trimmed from RNA-seq reads using
839 Trimmomatic (v0.3.9) (*Bolger et al., 2014*) with the following parameters:
840 *ILLUMINACLIP:TruSeq3-SE.fa:1:30:12*. Trimmed reads were aligned to the *C. elegans* genome
841 (ce11 release ws263) using STAR (v2.6.1a) (*Dobin et al., 2013*) with the following parameters (all
842 others default): *--outSAMunmapped Within --outMultimapperOrder Random --*
843 *outFilterMismatchNmax 33 --seedSearchStartLmax 33 --alignSJoverhangMin 8 --*
844 *outFilterScoreMinOverLread 0.3 --alignIntronMin 40 --alignIntronMax 2200 --varVCFfile --*
845 *outSAMattributes NH HI AS nM vG vA vW --waspOutputMode SAMtag*. The *--varVCFfile* and --
846 *waspOutputMode* parameters (as well as output attributes *vG*, *vA*, and *vW*) run the WASP (*van de*
847 *Geijn et al., 2015*) algorithm during alignment, identifying reads that cover single nucleotide
848 variants occurring in any of the four non-reference strains and determining whether the read
849 would map uniquely when containing both the reference and alternate alleles. This process
850 enables exclusion of reads that would be discarded when containing non-reference alleles but
851 included when containing reference alleles, allowing better comparison across strains. Single
852 nucleotide variants in any of the four non-N2 strains in the CeNDR (*Cook et al. 2017*) VCF
853 (WI.20180527.hard-filter.vcf) were masked by WASP by including the input *--varVCFfile* in
854 STAR.
855

856 Reads were assigned to genes and counted using an extension of the 'HTSeq-count' method
857 (*Anders et al., 2015*), wherein totals of all reads, all unique reads, and all reads passing WASP's
858 filter (aligning uniquely when containing either the reference allele or the alternate allele,
859 whichever was actually observed) mapping to each gene were returned. This was implemented
860 with a custom Python script using the *htseq* module (v0.11.3).
861
862 *Differential expression analysis*
863
864 Differential gene expression was analyzed in R (v4.0.3) (*R Core Team, 2020*) using the *DESeq2*
865 package (v1.28.1) (*Love et al., 2014*); effect sizes and p-values were corrected using the 'ashr'
866 method from the *ashr* package (v2.2-47) (*Stephens, 2017*). The counts for each gene were
867 modeled using the *DESeq2* negative binomial generalized linear model as follows:
868 $$\log2(q_{ij}) = \beta_i x_{j.} + \beta_i y_{j.},$$
869 where for gene *i,* sample *j, q* is proportional to the true concentration of RNA fragments for a
870 gene, with *q* derived from observed WASP-passing read counts per gene via negative binomial
871 gene-specific dispersion modeling including sample-specific size factors (*Love et al., 2014*). β_i
872 gives the log2 fold changes for gene *i*. *x* represents the biological replicate and *y* represents the
873 strain-treatment combination for the sample, with a total of 15 combinations: five strains by three
874 RNAi treatments, including the control.
875
876 Results were extracted as contrasts between the strain-treatment combinations of interest, e.g.
877 strain vs strain on the control condition, or treatment vs control for a single strain. Genes were
878 considered differentially expressed if their ashr-adjusted p-values were < 0.1. These adjusted p-
879 values represent FDRs that account for variance, initial effect size and the number of tests
880 performed. The effect sizes reported are ashr-adjusted log2 fold changes.
881
882 **Droplet digital PCR**
883
884 To design an unbiased primer set, we identified regions of identical sequence between *ppw-1* and
885 *sago-2* and across the ten strains of interest. Following (*Kamitaki et al., 2018*), we chose primers
886 to target both genes, and probes to discriminate between *ppw-1* (FAM) and *sago-2* (HEX).
887 Sequences are as follows: forward (CTTGGTACCGCTCCGCTC), reverse

888 (GCTGATTCGGTTTGATCGTC), *ppw-1* probe (AGACGAGAAATGTGGAGAGGGGAA),
889 *sago-2* probe (AGACGAGAAATGAGGAGTGGGGAA). Both probes anneal in the same
890 location, ensuring competition between them.
891
892 Worms from strains N2, CB4856, CB4852, DL238, ECA369, EG4348, JU1088, JU1581,
893 KR314, and QX1211 were reared under standard conditions (as above), bleached to isolate
894 embryos, and grown to reproductive maturity. RNA was extracted with TRIzol (Invitrogen
895 #15596026) and RNeasy columns (Qiagen #74104), following (*He, 2011*). RNA was collected at
896 two timepoints, early and middle reproductive maturity (68±2hrs and 90±2hrs after bleaching,
897 respectively). RNA sample concentrations were quantified and standardized using a Nanodrop
898 (Thermo Scientific), and cDNA was synthesized using the ProtoScript II First Stand cDNA
899 Synthesis Kit (NEB #E6560S). The experiment was replicated as follows: from each
900 experimental condition, we collected two RNA samples, for two biological replicates; within the
901 plate, each reaction was duplicated, for two technical replicates; and we conducted the entire
902 experiment twice.
903
904 Droplet digital PCR was carried out with the Bio-Rad QX200 system following the
905 manufacturer's protocol, and results were obtained using the QuantaSoft software (Bio-Rad), via
906 both automatic thresholding and manual droplet selection. All samples produced >8000 droplets
907 and results from all samples were retained. Concentration, given by number of copies per μL,
908 was modeled with a quasipoisson error structure using the *glm()* function in R. As *ppw-1* was
909 detected at an order of magnitude higher than *sago-2*, we analyzed the two genes separately. By
910 model selection, we identified the minimal model that best described the observed differences in
911 concentration For the *ppw-1* analysis, we dropped run date from the model, as it was not
912 significant; for *sago-2*, run date contributed <1% to the total observed deviance (Table S1), but
913 was nevertheless significant, so it was retained. The final models were: Concentration ~
914 Strain*DevStage/BiolRep for *ppw-1*, and Concentration ~ RunDate + Strain*DevStage/BiolRep
915 for *sago-2*. To determine which strains differed in *ppw-1* or *sago-2* levels, we performed
916 pairwise contrasts among strains using the *TukeyHSD()* function and a family-wise confidence
917 level of 95% (only a subset of comparisons are reported in the text). To determine which strains
918 showed differences in concentration according to developmental stage, we performed pairwise

919 contrasts using the *lsmeans()* function in the package *lsmeans*, using a confidence level of 95%
920 following a Bonferroni correction for multiple tests.
921
922 **Genotype and sequence analysis**
923
924 To evaluate population-level allelic variation at known RNAi genes, we queried the *C. elegans*
925 Natural Diversity Resource (https://elegansvariation.org), which provides genotype data for 403
926 wild isotypes from short read sequence data mapped to the N2 reference genome (*Cook et al.,*
927 *2017*). Specifically, we downloaded the VCF (WI.20200815.hard-filter.isotype.vcf) and used the
928 R package *VariantAnnotation* (*Obenchain et al., 2014*) to extract information about mutations and
929 mapping coverage, and the package *PopGenome* (*Pfeifer et al., 2014*) to estimate nucleotide
930 diversity, at each gene. Haplotype networks for individual genes were determined using the R
931 package *pegas* (*Paradis, 2010*).
932
933 For a subset of strains, we verified and/or supplemented the genotype data with de novo-
934 assembled genome data and long read data. Genomic DNA of strains AB2, EG4347, EG4348,
935 JU1088, JU1171, PB306, PX174, QX1211 and QX1216 was prepared using standard
936 phenol/chloroform extraction and ethanol precipitation. Samples were cleaned with DNA Clean
937 & Concentrator columns (Zymo Research #D4004) and libraries were prepared using NEBNext
938 Ultra II FS DNA Library Prep Kit for Illumina (New England Biolabs #E7805) and Multiplex
939 Oligos for Illumina (NEB #E7500), with customized fragmentation and purification steps to
940 enrich for desired sizes. A final DNA size selection targeting 650bp±50bp was performed using
941 BluePippin (Sage Science). The libraries were sequenced on a HiSeq 2500 (Illumina) on Rapid
942 Run Mode (paired-end 2x250bp) in the Molecular Evolution Core at the Georgia Institute of
943 Technology. Raw data were trimmed using Cutadapt (v1.18) (*Martin, 2011*) and quality control
944 was performed with FastQC (*Andrews, 2021*). Reads were then assembled into contigs with
945 DISCOVAR *de novo* (v52488) (Broad Institute) using default parameters. Separately, QX1211
946 and JU1088 genomic DNA samples were snap frozen with liquid nitrogen and sent to the
947 Georgia Genomics and Bioinformatics Core (GGBC) at the University of Georgia. Quality was
948 assessed by Qubit (Invitrogen) and NanoDrop (Thermo Scientific), molecular weight distribution
949 was assessed by fragment analysis, and sizes >15kb were selected by BluePippin (Sage Science).
950 Each sample was sequenced on a single SMRT Cell on the PacBio Sequel I platform (Pacific

951 Biosciences). Genome assembly was performed by the GGBC using Canu (v1.7) (*Koren et al.,*
952 *2017*).
953
954 **Computing**
955
956 Unless otherwise specified, all analyses were performed in R (*R Core Team, 2020*) and figures
957 were generated with the packages *ggplot2* (*Wickham, 2016*) and *ggpubr* (*Kassambara, 2020*).
958 Computationally intensive jobs, including read mapping and genome assembly, were performed
959 on PACE, the high performance computing platform at the Georgia Institute of Technology.
960
961 **ACKNOWLEDGEMENTS**
962
963 We wish to acknowledge the core facilities at the Parker H. Petit Institute for Bioengineering and
964 Bioscience at the Georgia Institute of Technology for the use of their shared equipment, services
965 and expertise. Specifically, we are grateful to Aaron Lifland at the Optimal Microscopy Core for
966 training in confocal imaging, and Anton Bryksin, Naima Djeddar, and Shweta Biliya at the
967 Molecular Evolution Core for collaboration on the sequencing projects. We also thank the
968 Georgia Genomics and Bioinformatics Core at the University of Georgia for PacBio sequencing
969 and genome assembly. We thank Miyeko Mana for the gift of the *par-4* RNAi clone, and Lijiang
970 Long and Patrick McGrath for strain PTM377. Some strains were provided by the CGC, which is
971 funded by NIH Office of Research Infrastructure Programs (P40 OD010440). This research was
972 supported in part through research cyberinfrastructure resources and services provided by the
973 Partnership for an Advanced Computing Environment (PACE) at the Georgia Institute of
974 Technology. This research was funded by NIH grant R35 GM119744 to A.B.P. and NSF grant
975 MCB1518314 to D.A.P.
976
977 **LITERATURE CITED**
978
979 Ahringer, J. (2006). Reverse genetics. In *WormBook: The Online Review of C. elegans Biology [Internet]*.
980 WormBook. https://www.ncbi.nlm.nih.gov/books/NBK19711/

981 Anders, S., Pyl, P. T., & Huber, W. (2015). HTSeq—A Python framework to work with high-throughput
982 sequencing data. *Bioinformatics (Oxford, England)*, *31*(2), 166–169.
983 https://doi.org/10.1093/bioinformatics/btu638

984 Andersen, E. C., Gerke, J. P., Shapiro, J. A., Crissman, J. R., Ghosh, R., Bloom, J. S., Félix, M.-A., &
985 Kruglyak, L. (2012). Chromosome-scale selective sweeps shape Caenorhabditis elegans genomic
986 diversity. *Nature Genetics*, *44*(3), 285–290. https://doi.org/10.1038/ng.1050

987 Andrews, S. (2021). *FastQC: A quality control tool for high throughput sequence data*.
988 https://www.bioinformatics.babraham.ac.uk/projects/fastqc/

989 Ashe, A., Bélicard, T., Le Pen, J., Sarkies, P., Frézal, L., Lehrbach, N. J., Félix, M.-A., & Miska, E. A.
990 (2013). A deletion polymorphism in the Caenorhabditis elegans RIG-I homolog disables viral RNA
991 dicing and antiviral immunity. *ELife*, *2*, e00994. https://doi.org/10.7554/eLife.00994

992 Ashe, A., Sarkies, P., Le Pen, J., Tanguy, M., & Miska, E. A. (2015). Antiviral RNA Interference against
993 Orsay Virus Is neither Systemic nor Transgenerational in Caenorhabditis elegans. *Journal of*
994 *Virology*, *89*(23), 12035–12046. https://doi.org/10.1128/JVI.03664-14

995 Ben-David, E., Burga, A., & Kruglyak, L. (2017). A maternal-effect selfish genetic element in
996 Caenorhabditis elegans. *Science (New York, N.Y.)*, *356*(6342), 1051–1055.
997 https://doi.org/10.1126/science.aan0621

998 Billi, A. C., Fischer, S. E. J., & Kim, J. K. (2014). Endogenous RNAi pathways in C. elegans.
999 *WormBook: The Online Review of C. Elegans Biology*, 1–49.
1000 https://doi.org/10.1895/wormbook.1.170.1

1001 Bolger, A. M., Lohse, M., & Usadel, B. (2014). Trimmomatic: A flexible trimmer for Illumina sequence
1002 data. *Bioinformatics (Oxford, England)*, *30*(15), 2114–2120.
1003 https://doi.org/10.1093/bioinformatics/btu170

1004 Buck, A. H., & Blaxter, M. (2013). Functional diversification of Argonautes in nematodes: An expanding
1005 universe. *Biochemical Society Transactions*, *41*(4), 881–886. https://doi.org/10.1042/BST20130086

1006 Campbell, R. F., McGrath, P. T., & Paaby, A. B. (2018). Analysis of Epistasis in Natural Traits Using
1007 Model Organisms. *Trends in Genetics: TIG*, *34*(11), 883–898.
1008 https://doi.org/10.1016/j.tig.2018.08.002

1009 Chandler, C. H., Chari, S., & Dworkin, I. (2013). Does your gene need a background check? How genetic
1010 background impacts the analysis of mutations, genes, and evolution. *Trends in Genetics: TIG*, *29*(6),
1011 358–366. https://doi.org/10.1016/j.tig.2013.01.009

1012 Charles, S., Aubry, G., Chou, H.-T., Paaby, A. B., & Lu, H. (2021). High-Temporal-Resolution smFISH
1013 Method for Gene Expression Studies in Caenorhabditis elegans Embryos. *Analytical Chemistry*,
1014 *93*(3), 1369–1376. https://doi.org/10.1021/acs.analchem.0c02966

1015 Cook, D. E., Zdraljevic, S., Roberts, J. P., & Andersen, E. C. (2017). CeNDR, the Caenorhabditis elegans
1016 natural diversity resource. *Nucleic Acids Research*, *45*(D1), D650–D657.
1017 https://doi.org/10.1093/nar/gkw893

1018 Crombie, T. A., Zdraljevic, S., Cook, D. E., Tanny, R. E., Brady, S. C., Wang, Y., Evans, K. S., Hahnel,
1019 S., Lee, D., Rodriguez, B. C., Zhang, G., van der Zwagg, J., Kiontke, K., & Andersen, E. C. (2019).
1020 Deep sampling of Hawaiian Caenorhabditis elegans reveals high genetic diversity and admixture
1021 with global populations. *ELife*, *8*, e50465. https://doi.org/10.7554/eLife.50465

1022 Dalzell, J. J., McVeigh, P., Warnock, N. D., Mitreva, M., Bird, D. M., Abad, P., Fleming, C. C., Day, T.
1023 A., Mousley, A., Marks, N. J., & Maule, A. G. (2011). RNAi effector diversity in nematodes. *PLoS*
1024 *Neglected Tropical Diseases*, *5*(6), e1176. https://doi.org/10.1371/journal.pntd.0001176

1025 De-Souza, E. A., Camara, H., Salgueiro, W. G., Moro, R. P., Knittel, T. L., Tonon, G., Pinto, S., Pinca, A.
1026 P. F., Antebi, A., Pasquinelli, A. E., Massirer, K. B., & Mori, M. A. (2019). RNA interference may
1027 result in unexpected phenotypes in Caenorhabditis elegans. *Nucleic Acids Research*, *47*(8), 3957–
1028 3969. https://doi.org/10.1093/nar/gkz154

1029 Dobin, A., Davis, C. A., Schlesinger, F., Drenkow, J., Zaleski, C., Jha, S., Batut, P., Chaisson, M., &
1030 Gingeras, T. R. (2013). STAR: Ultrafast universal RNA-seq aligner. *Bioinformatics*, *29*(1), 15–21.
1031 https://doi.org/10.1093/bioinformatics/bts635

1032 Elvin, M., Snoek, L. B., Frejno, M., Klemstein, U., Kammenga, J. E., & Poulin, G. B. (2011). A fitness
1033 assay for comparing RNAi effects across multiple C. elegans genotypes. *BMC Genomics*, *12*, 510.
1034 https://doi.org/10.1186/1471-2164-12-510

1035 Félix, M.-A. (2008). RNA interference in nematodes and the chance that favored Sydney Brenner.
1036 *Journal of Biology*, *7*(9), 34. https://doi.org/10.1186/jbiol97

1037 Félix, M.-A., Ashe, A., Piffaretti, J., Wu, G., Nuez, I., Bélicard, T., Jiang, Y., Zhao, G., Franz, C. J.,
1038 Goldstein, L. D., Sanroman, M., Miska, E. A., & Wang, D. (2011). Natural and experimental
1039 infection of Caenorhabditis nematodes by novel viruses related to nodaviruses. *PLoS Biology*, *9*(1),
1040 e1000586. https://doi.org/10.1371/journal.pbio.1000586

1041 Fire, A., Xu, S., Montgomery, M. K., Kostas, S. A., Driver, S. E., & Mello, C. C. (1998). Potent and
1042 specific genetic interference by double-stranded RNA in Caenorhabditis elegans. *Nature*,
1043 *391*(6669), 806–811. https://doi.org/10.1038/35888

1044 Franz, C. J., Renshaw, H., Frezal, L., Jiang, Y., Félix, M.-A., & Wang, D. (2014). Orsay, Santeuil and Le
1045 Blanc viruses primarily infect intestinal cells in Caenorhabditis nematodes. *Virology*, *448*, 255–264.
1046 https://doi.org/10.1016/j.virol.2013.09.024

1047 Frézal, L., Demoinet, E., Braendle, C., Miska, E., & Félix, M.-A. (2018). Natural genetic variation in a
1048 multigenerational phenotype in C. elegans. *Current Biology : CB*, *28*(16), 2588-2596.e8.
1049 https://doi.org/10.1016/j.cub.2018.05.091

1050 Grishok, A. (2013). Biology and Mechanisms of Short RNAs in Caenorhabditis elegans. *Advances in*
1051 *Genetics*, *83*, 1–69. https://doi.org/10.1016/B978-0-12-407675-4.00001-8

1052 Harris, T. W., Arnaboldi, V., Cain, S., Chan, J., Chen, W. J., Cho, J., Davis, P., Gao, S., Grove, C. A.,
1053 Kishore, R., Lee, R. Y. N., Muller, H.-M., Nakamura, C., Nuin, P., Paulini, M., Raciti, D., Rodgers,
1054 F. H., Russell, M., Schindelman, G., … Sternberg, P. W. (2020). WormBase: A modern Model
1055 Organism Information Resource. *Nucleic Acids Research*, *48*(D1), D762–D767.
1056 https://doi.org/10.1093/nar/gkz920

1057 He, F. (2011). Total RNA Extraction from C. elegans. *Bio-Protocol*, e47–e47.

1058 Hodgkin, J., & Doniach, T. (1997). Natural variation and copulatory plug formation in Caenorhabditis
1059 elegans. *Genetics*, *146*(1), 149–164.

1060 Hothorn, T., Bretz, F., & Westfall, P. (2008). Simultaneous inference in general parametric models.
1061 *Biometrical Journal. Biometrische Zeitschrift*, *50*(3), 346–363.
1062 https://doi.org/10.1002/bimj.200810425

1063 Houri-Zeevi, L., Korem Kohanim, Y., Antonova, O., & Rechavi, O. (2020). Three Rules Explain
1064 Transgenerational Small RNA Inheritance in C. elegans. *Cell*, *182*(5), 1186-1197.e12.
1065 https://doi.org/10.1016/j.cell.2020.07.022

Houri-Zeevi, L., Teichman, G., Gingold, H., & Rechavi, O. (2021). Stress resets ancestral heritable small RNA responses. *ELife*, *10*, e65797. https://doi.org/10.7554/eLife.65797

Kamath, R. S., & Ahringer, J. (2003). Genome-wide RNAi screening in Caenorhabditis elegans. *Methods (San Diego, Calif.)*, *30*(4), 313–321. https://doi.org/10.1016/s1046-2023(03)00050-1

Kamath, R. S., Fraser, A. G., Dong, Y., Poulin, G., Durbin, R., Gotta, M., Kanapin, A., Le Bot, N., Moreno, S., Sohrmann, M., Welchman, D. P., Zipperlen, P., & Ahringer, J. (2003). Systematic functional analysis of the Caenorhabditis elegans genome using RNAi. *Nature*, *421*(6920), 231–237. https://doi.org/10.1038/nature01278

Kamath, R. S., Martinez-Campos, M., Zipperlen, P., Fraser, A. G., & Ahringer, J. (2001). Effectiveness of specific RNA-mediated interference through ingested double-stranded RNA in Caenorhabditis elegans. *Genome Biology*, *2*(1), RESEARCH0002. https://doi.org/10.1186/gb-2000-2-1-research0002

Kamitaki, N., Usher, C. L., & McCarroll, S. A. (2018). Using Droplet Digital PCR to Analyze Allele-Specific RNA Expression. *Methods in Molecular Biology (Clifton, N.J.)*, *1768*, 401–422. https://doi.org/10.1007/978-1-4939-7778-9_23

Kassambara, A. (2020). *ggpubr: "ggplot2" Based Publication Ready Plots*. https://rpkgs.datanovia.com/ggpubr/

Koren, S., Walenz, B. P., Berlin, K., Miller, J. R., Bergman, N. H., & Phillippy, A. M. (2017). Canu: Scalable and accurate long-read assembly via adaptive k-mer weighting and repeat separation. *Genome Research*, *27*(5), 722–736. https://doi.org/10.1101/gr.215087.116

Lee, D., Zdraljevic, S., Stevens, L., Wang, Y., Tanny, R. E., Crombie, T. A., Cook, D. E., Webster, A. K., Chirakar, R., Baugh, L. R., Sterken, M. G., Braendle, C., Félix, M.-A., Rockman, M. V., & Andersen, E. C. (2021). Balancing selection maintains hyper-divergent haplotypes in Caenorhabditis elegans. *Nature Ecology & Evolution*, *5*(6), 794–807. https://doi.org/10.1038/s41559-021-01435-x

Love, M. I., Huber, W., & Anders, S. (2014). Moderated estimation of fold change and dispersion for RNA-seq data with DESeq2. *Genome Biology*, *15*(12), 550. https://doi.org/10.1186/s13059-014-0550-8

Lüdecke, D. (2018). *sjstats: Statistical Functions for Regression Models.* Zenodo. https://doi.org/10.5281/zenodo.1489175

Martin, M. (2011). Cutadapt removes adapter sequences from high-throughput sequencing reads. *EMBnet.Journal*, *17*(1), 10–12. https://doi.org/10.14806/ej.17.1.200

Nuez, I., & Félix, M.-A. (2012). Evolution of susceptibility to ingested double-stranded RNAs in Caenorhabditis nematodes. *PloS One*, *7*(1), e29811. https://doi.org/10.1371/journal.pone.0029811

Obbard, D. J., Gordon, K. H. J., Buck, A. H., & Jiggins, F. M. (2009). The evolution of RNAi as a defence against viruses and transposable elements. *Philosophical Transactions of the Royal Society B: Biological Sciences*, *364*(1513), 99–115. https://doi.org/10.1098/rstb.2008.0168

Obenchain, V., Lawrence, M., Carey, V., Gogarten, S., Shannon, P., & Morgan, M. (2014). VariantAnnotation: A Bioconductor package for exploration and annotation of genetic variants. *Bioinformatics (Oxford, England)*, *30*(14), 2076–2078. https://doi.org/10.1093/bioinformatics/btu168

Paaby, A. B., & Testa, N. D. (2018). Developmental Plasticity and Evolution. In L. Nuno de la Rosa & G. Müller (Eds.), *Evolutionary Developmental Biology: A Reference Guide* (pp. 1–14). Springer International Publishing. https://doi.org/10.1007/978-3-319-33038-9_110-1

Paaby, A. B., White, A. G., Riccardi, D. D., Gunsalus, K. C., Piano, F., & Rockman, M. V. (2015). Wild worm embryogenesis harbors ubiquitous polygenic modifier variation. *ELife*, *4*. https://doi.org/10.7554/eLife.09178

Pagliuso, D. C., Bodas, D. M., & Pasquinelli, A. E. (2021). Recovery from heat shock requires the microRNA pathway in Caenorhabditis elegans. *PLOS Genetics*, *17*(8), e1009734. https://doi.org/10.1371/journal.pgen.1009734

Paradis, E. (2010). pegas: An R package for population genetics with an integrated-modular approach. *Bioinformatics (Oxford, England)*, *26*(3), 419–420. https://doi.org/10.1093/bioinformatics/btp696

Pfeifer, B., Wittelsbürger, U., Ramos-Onsins, S. E., & Lercher, M. J. (2014). PopGenome: An efficient Swiss army knife for population genomic analyses in R. *Molecular Biology and Evolution*, *31*(7), 1929–1936. https://doi.org/10.1093/molbev/msu136

Pollard, D. A., & Rockman, M. V. (2013). Resistance to germline RNA interference in a Caenorhabditis elegans wild isolate exhibits complexity and nonadditivity. *G3 (Bethesda, Md.)*, *3*(6), 941–947. https://doi.org/10.1534/g3.113.005785

R Core Team. (2020). *R: A language and environment for statistical computing*. R Foundation for Statistical Computing. https://www.R-project.org/

Raj, A., van den Bogaard, P., Rifkin, S. A., van Oudenaarden, A., & Tyagi, S. (2008). Imaging individual mRNA molecules using multiple singly labeled probes. *Nature Methods*, *5*(10), 877–879. https://doi.org/10.1038/nmeth.1253

Richaud, A., Frézal, L., Tahan, S., Jiang, H., Blatter, J. A., Zhao, G., Kaur, T., Wang, D., & Félix, M.-A. (2019). Vertical transmission in Caenorhabditis nematodes of RNA molecules encoding a viral RNA-dependent RNA polymerase. *Proceedings of the National Academy of Sciences of the United States of America*, *116*(49), 24738–24747. https://doi.org/10.1073/pnas.1903903116

Rual, J.-F., Ceron, J., Koreth, J., Hao, T., Nicot, A.-S., Hirozane-Kishikawa, T., Vandenhaute, J., Orkin, S. H., Hill, D. E., van den Heuvel, S., & Vidal, M. (2004). Toward improving Caenorhabditis elegans phenome mapping with an ORFeome-based RNAi library. *Genome Research*, *14*(10B), 2162–2168. https://doi.org/10.1101/gr.2505604

Sarkies, P., Ashe, A., Le Pen, J., McKie, M. A., & Miska, E. A. (2013). Competition between virus-derived and endogenous small RNAs regulates gene expression in Caenorhabditis elegans. *Genome Research*, *23*(8), 1258–1270. https://doi.org/10.1101/gr.153296.112

Schindelin, J., Arganda-Carreras, I., Frise, E., Kaynig, V., Longair, M., Pietzsch, T., Preibisch, S., Rueden, C., Saalfeld, S., Schmid, B., Tinevez, J.-Y., White, D. J., Hartenstein, V., Eliceiri, K., Tomancak, P., & Cardona, A. (2012). Fiji: An open-source platform for biological-image analysis. *Nature Methods*, *9*(7), 676–682. https://doi.org/10.1038/nmeth.2019

Schneider, C. A., Rasband, W. S., & Eliceiri, K. W. (2012). NIH Image to ImageJ: 25 years of image analysis. *Nature Methods*, *9*(7), 671–675. https://doi.org/10.1038/nmeth.2089

Schott, D. H., Cureton, D. K., Whelan, S. P., & Hunter, C. P. (2005). An antiviral role for the RNA interference machinery in Caenorhabditis elegans. *Proceedings of the National Academy of Sciences of the United States of America*, *102*(51), 18420–18424. https://doi.org/10.1073/pnas.0507123102

Seidel, H. S., Ailion, M., Li, J., van Oudenaarden, A., Rockman, M. V., & Kruglyak, L. (2011). A novel sperm-delivered toxin causes late-stage embryo lethality and transmission ratio distortion in C. elegans. *PLoS Biology*, *9*(7), e1001115. https://doi.org/10.1371/journal.pbio.1001115

Seidel, H. S., Rockman, M. V., & Kruglyak, L. (2008). Widespread genetic incompatibility in C. elegans maintained by balancing selection. *Science (New York, N.Y.)*, *319*(5863), 589–594. https://doi.org/10.1126/science.1151107

Shabalina, S. A., & Koonin, E. V. (2008). Origins and evolution of eukaryotic RNA interference. *Trends in Ecology & Evolution*, *23*(10), 578–587. https://doi.org/10.1016/j.tree.2008.06.005

Shiu, P. K., & Hunter, C. P. (2017). Early Developmental Exposure to dsRNA Is Critical for Initiating Efficient Nuclear RNAi in C. elegans. *Cell Reports*, *18*(12), 2969–2978. https://doi.org/10.1016/j.celrep.2017.03.002

Stephens, M. (2017). False discovery rates: A new deal. *Biostatistics (Oxford, England)*, *18*(2), 275–294. https://doi.org/10.1093/biostatistics/kxw041

Stiernagle, T. (2006). Maintenance of C. elegans. *WormBook: The Online Review of C. Elegans Biology*, 1–11. https://doi.org/10.1895/wormbook.1.101.1

Testa, N. D., Kaul, S., Le, K. N., Zhan, M., Lu, H., & Paaby, A. B. (2020). A portable, low-cost device for precise control of specimen temperature under stereomicroscopes. *PloS One*, *15*(3), e0230241. https://doi.org/10.1371/journal.pone.0230241

Tijsterman, M., Okihara, K. L., Thijssen, K., & Plasterk, R. H. A. (2002). PPW-1, a PAZ/PIWI protein required for efficient germline RNAi, is defective in a natural isolate of C. elegans. *Current Biology: CB*, *12*(17), 1535–1540. https://doi.org/10.1016/s0960-9822(02)01110-7

Timmons, L., Court, D. L., & Fire, A. (2001). Ingestion of bacterially expressed dsRNAs can produce specific and potent genetic interference in Caenorhabditis elegans. *Gene*, *263*(1–2), 103–112. https://doi.org/10.1016/s0378-1119(00)00579-5

Timmons, L., & Fire, A. (1998). Specific interference by ingested dsRNA. *Nature*, *395*(6705), 854. https://doi.org/10.1038/27579

van de Geijn, B., McVicker, G., Gilad, Y., & Pritchard, J. K. (2015). WASP: Allele-specific software for robust molecular quantitative trait locus discovery. *Nature Methods*, *12*(11), 1061–1063. https://doi.org/10.1038/nmeth.3582

Wickham, H. (2016). *ggplot2: Elegant Graphics for Data Analysis*. Springer-Verlag. http://ggplot2.org

Wilkins, C., Dishongh, R., Moore, S. C., Whitt, M. A., Chow, M., & Machaca, K. (2005). RNA interference is an antiviral defence mechanism in Caenorhabditis elegans. *Nature*, *436*(7053), 1044–1047. https://doi.org/10.1038/nature03957

Wilson, R. C., & Doudna, J. A. (2013). Molecular Mechanisms of RNA Interference. *Annual Review of Biophysics*, *42*(1), 217–239. https://doi.org/10.1146/annurev-biophys-083012-130404

Winston, W. M., Sutherlin, M., Wright, A. J., Feinberg, E. H., & Hunter, C. P. (2007). Caenorhabditis elegans SID-2 is required for environmental RNA interference. *Proceedings of the National Academy of Sciences of the United States of America*, *104*(25), 10565–10570. https://doi.org/10.1073/pnas.0611282104

1188 Wu, A. C.-Y., & Rifkin, S. A. (2015). Aro: A machine learning approach to identifying single molecules
1189 and estimating classification error in fluorescence microscopy images. *BMC Bioinformatics*, *16*,
1190 102. https://doi.org/10.1186/s12859-015-0534-z

1191 Wynant, N., Santos, D., & Vanden Broeck, J. (2017). The evolution of animal Argonautes: Evidence for
1192 the absence of antiviral AGO Argonautes in vertebrates. *Scientific Reports*, *7*(1), 9230.
1193 https://doi.org/10.1038/s41598-017-08043-5

1194 Yigit, E. (2007). *The Argonaute Family of Genes in Caenorhabditis Elegans: A Dissertation*. University
1195 of Massachusetts Medical School.

1196 Yigit, E., Batista, P. J., Bei, Y., Pang, K. M., Chen, C.-C. G., Tolia, N. H., Joshua-Tor, L., Mitani, S.,
1197 Simard, M. J., & Mello, C. C. (2006). Analysis of the C. elegans Argonaute Family Reveals that
1198 Distinct Argonautes Act Sequentially during RNAi. *Cell*, *127*(4), 747–757.
1199 https://doi.org/10.1016/j.cell.2006.09.033

1200 Youngman, E. M., & Claycomb, J. M. (2014). From early lessons to new frontiers: The worm as a
1201 treasure trove of small RNA biology. *Frontiers in Genetics*, *5*, 416.
1202 https://doi.org/10.3389/fgene.2014.00416

1203

SUPPLEMENTAL FIGURES & TABLES

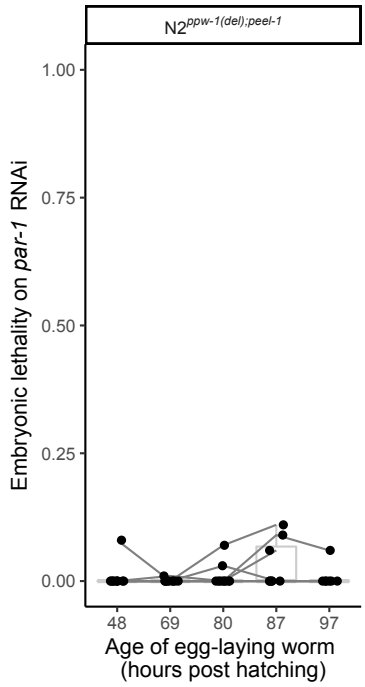

Figure S1. Embryonic lethality following RNAi against *par-1*.

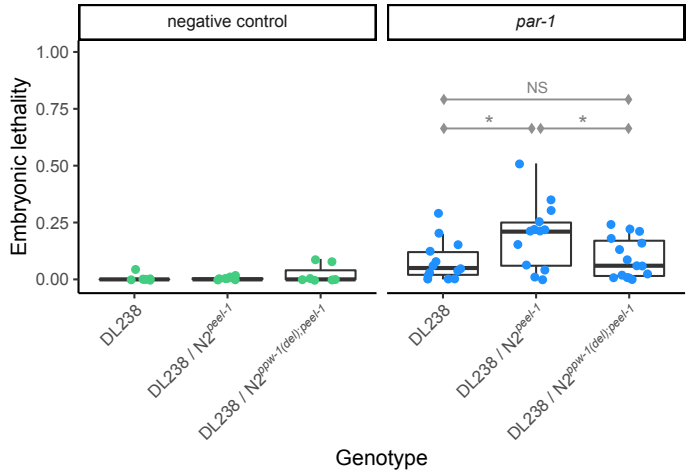

Figure S2. Complementation test for DL238 and the RNAi-sensitive laboratory strain N2, with and without a deletion allele at *ppw-1*. The embryos scored here were laid by pooled hermaphrodites on replicate plates. Significance level (Tukey's contrasts): $p<0.05$ (*).

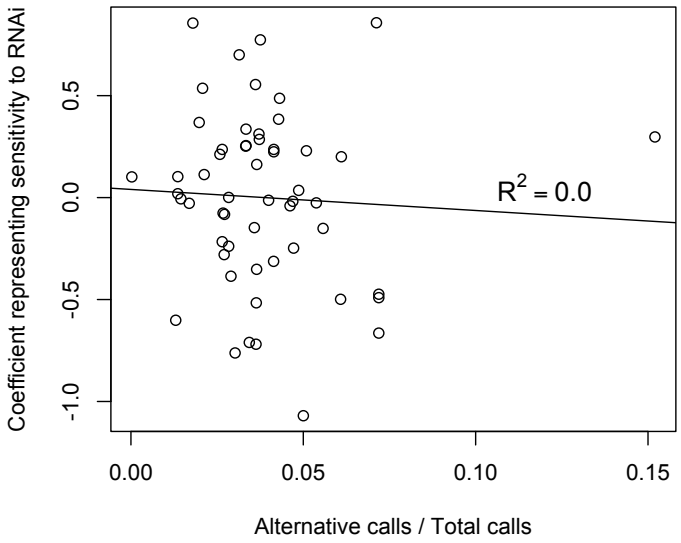

Figure S3. RNAi sensitivity for 55 wild isolates, versus genetic distance from the reference strain N2. RNAi data is from (*Paaby et al., 2015*), which measured embryonic lethality following RNAi by feeding against 29 individual maternal-effect targets. The y-axis plots the coefficients associated with the strain term in the full statistical model, and represents the strain-specific variation in embryonic lethality associated with RNAi responsiveness; increasingly positive values indicate weaker germline RNAi (*Paaby et al., 2015*). The x-axis gives the proportion of alternate genotype calls, out of the total number of calls, for each strain in the CeNDR database (*Cook et al., 2017*).

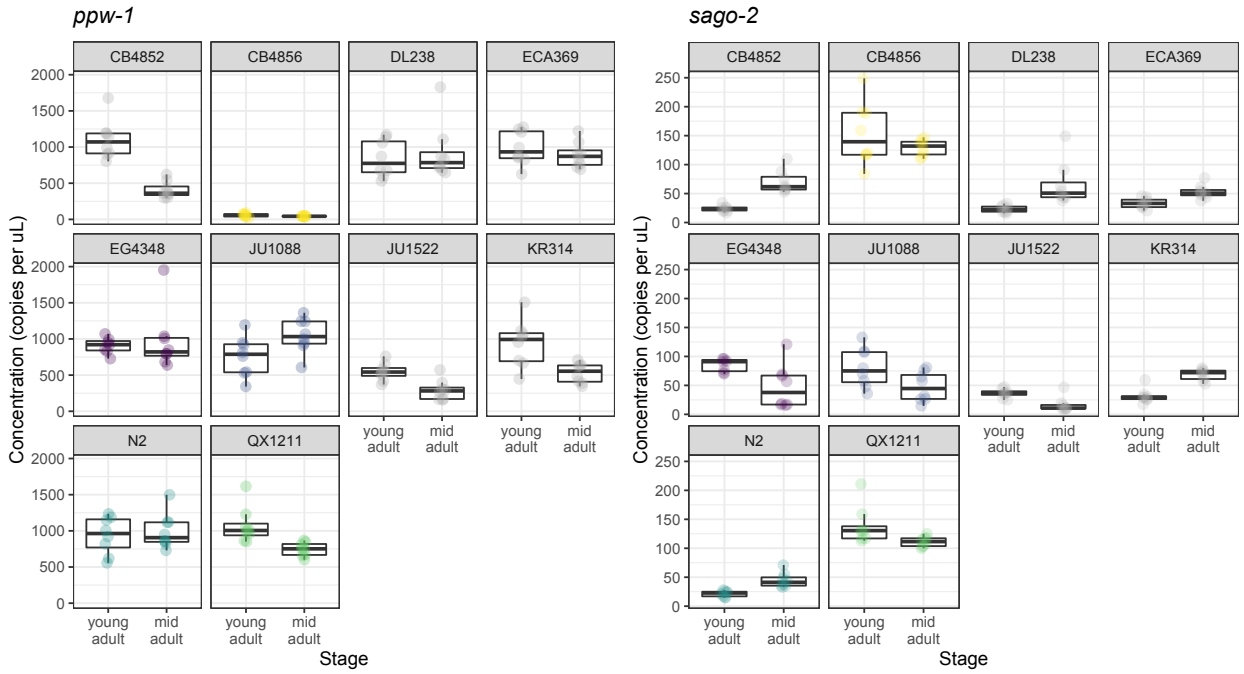

Figure S4. Droplet digital PCR results for *ppw-1* and *sago-2* for all ten tested strains. Colors correspond to strains also evaluated by RNA-seq (Figure 6).

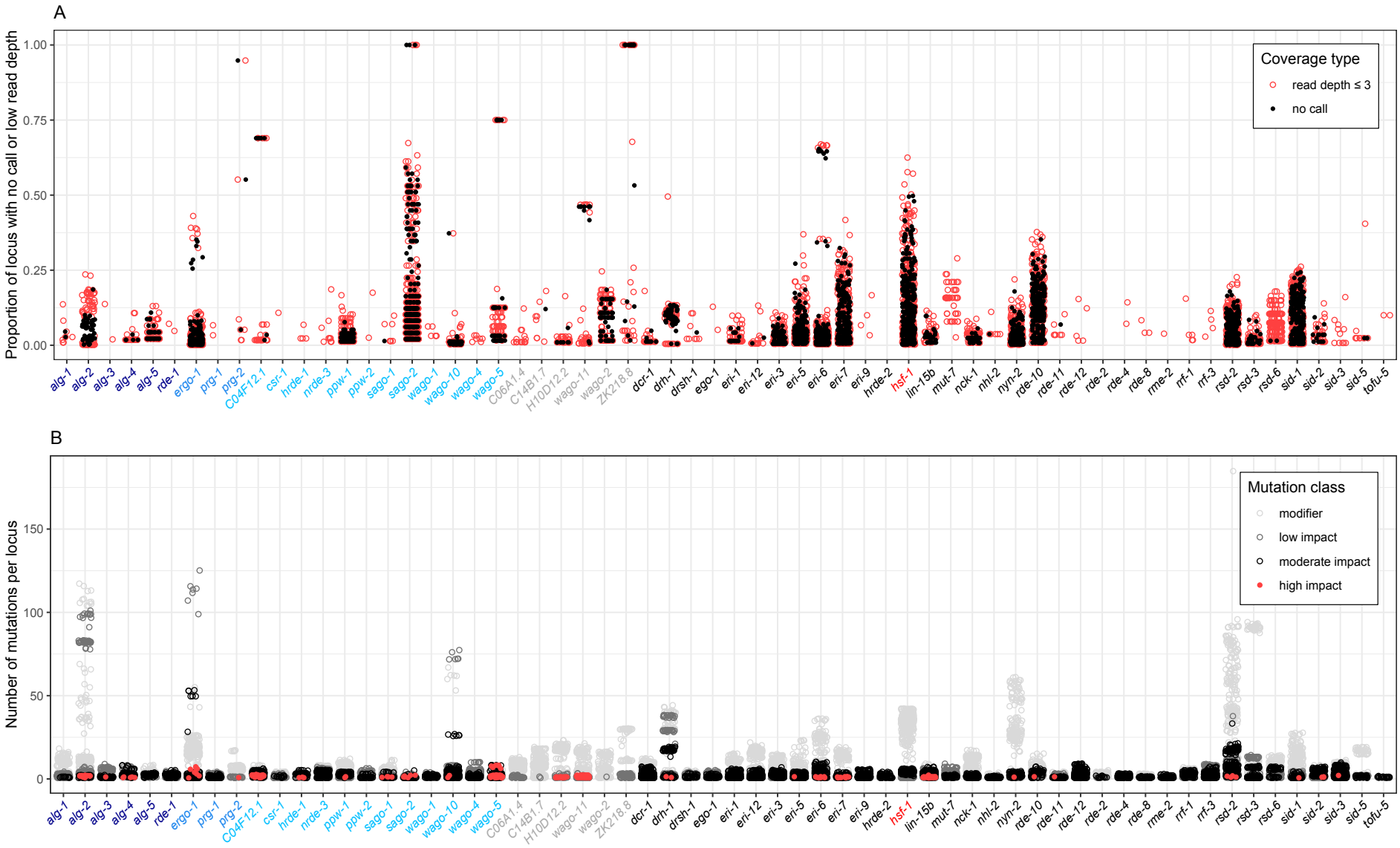

Figure S5. For 62 RNAi genes, mapping coverage (A) and mutational variation (B) in the 403 strain isotypes from CeNDR. Gene names are color coded by classification: AGO Argonaute (dark blue), PIWI Argonaute (blue), WAGO Argonaute (light blue), Argonaute pseudogenes (grey), and other RNAi factor (black or red). Each point corresponds to an individual strain; zeros (no observation of poor coverage or mutation relative to the reference) are not plotted.

Table S1. Statistical results for the ddPCR analysis. The model used for each gene is described in the Methods.

ppw-1

	Df	Deviance	Resid. Df	Resid. Dev
NULL			158	37942
Strain	9	24433.1	149	13509
DevStage	1	910.3	148	12599
Strain:DevStage	9	4271.9	139	8327
Strain:DevStage:BiolRepl	20	2327.6	119	5999

sago-2

	Df	Deviance	Resid. DF	Resid. Dev
NULL			158	4722.0
RunDate	1	29.38	157	4692.6
Strain	9	2932.73	148	1759.9
DevStage	1	5.87	147	1754.0
Strain:DevStage	9	825.20	138	928.8
Strain:DevStage:BiolRepl	20	436.26	118	492.6

Table S2. Candidate genes for weak germline RNAi in the seven strains tested. Only genes with relevant genotypes in at least one strain are displayed, out of 62 RNAi genes queried. "High impact" indicates disruptive mutations like frameshifts or stop-gains. "Poor mapping coverage" indicates a read depth of 3 or less. "Functional diverged allele" indicates at least 1% nucleotide divergence from the reference genome, including at least five moderate mutations, such as amino acid substitutions, and no high impact mutations.

Class	Gene	One or more high impact mutation	Poor mapping coverage at 10% or more of locus	Functional diverged allele
Argonaute (AGO)	*alg-4*			QX1211
Argonaute (PIWI)	*ergo-1*	ECA369	ECA369	
Argonaute (WAGO)	*hrde-1*			QX1211
	nrde-3			QX1211
	ppw-1	CB4856		
	sago-2	DL238	DL238, ECA369, JU1522, KR314, QX1211	
	wago-10			QX1211
Argonaute (pseudogene)	*wago-11*	CB4852, KR314, QX1211	CB4856	
	wago-2		QX1211	
	ZK218.8		DL238	
Other RNAi factor	*dcr-1*			QX1211
	drh-1			QX1211
	eri-1			QX1211
	eri-5		JU1522	
	eri-6			QX1211
	eri-7	CB4856, DL238, ECA369	DL238, JU1522, KR314	
	eri-9			QX1211
	lin-15b	QX1211		ECA369
	nyn-2		DL238	QX1211
	rde-10		DL238, ECA369, JU1522, KR314, QX1211	
	rde-12			QX1211
	rsd-2		JU1522, QX1211	CB4856, DL238, ECA369, QX1211
	sid-1		DL238, ECA369, JU1522, QX1211	
	sid-2			QX1211
	sid-3			QX1211
	hsf-1		DL238, ECA369, JU1522, KR314	ECA369, KR314

Table S3. Strains used in this study.

Ref in text	Name	Genotype	Provenance
CB4852	CB4852	wild-type	Gift from Matthew Rockman
CB4856	CB4856	wild-type	Gift from Matthew Rockman
DL238	DL238	wild-type	Gift from Matthew Rockman
ECA369	ECA369	wild-type	Purchased from CeNDR
ECA701	ECA701	wild-type	Purchased from CeNDR
KR314	KR314	wild-type	Gift from Matthew Rockman
EG4348	EG4348	wild-type	Gift from Matthew Rockman
JU561	JU561	wild-type	Purchased from CeNDR
JU1088	JU1088	wild-type	Gift from Matthew Rockman
JU1522	JU1522	wild-type	Gift from Matthew Rockman
N2	N2	wild-type	Gift from Matthew Rockman
N2^{peel-1}	PTM377	*peel-1*(*kah126*) I	Gift from Patrick McGrath
N2^{ppw-1}	QF201	*ppw-1*(*pk1425*) I	Derived from backcrossing strain NL3511 5x to N2
N2$^{ppw-1;peel-1}$	QF204	*ppw-1*(*pk1425*) *peel-1*(*kah126*) I	Derived from PTM377 and QF201
N2$^{ppw-1\ CB4856}$	NL2550	*ppw-1*(*pk2505*) I	Purchased from CGC
NL3511	NL3511	*ppw-1*(*pk1425*) I	Purchased from CGC
QF14	QF14	*zuIs178*; *stIs10024 [RW10029>CB4856]*	Derived from backcrossing strain RW10029 18x to CB4856
QF15	QF15	*zuIs178; stIs10024 [RW10029>JU1522]*	Derived from backcrossing strain RW10029 16x to JU1522
QF16	QF16	*zuIs178*; *stIs10024 [RW10029>ECA369]*	Derived from backcrossing strain RW10029 17x to ECA369
QF90	QF90	*zuIs178*; *stIs10024 [RW10029>QX1211]*	Derived from backcrossing strain RW10029 10x to QX1211
QX1211	QX1211	wild-type	Gift from Matthew Rockman
RW10029	RW10029	*zuIs178*; *stIs10024*	Purchased from CGC
XZ1516	XZ1516	wild-type	Purchased from CeNDR